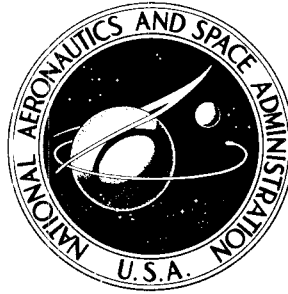


**NASA TECHNICAL
MEMORANDUM**



NASA TM X-2843

NASA TM X-2843

**CASE FILE
COPY**

**A COMPUTER PROGRAM FOR CALCULATING
THE PERFECT GAS INVISCID FLOW FIELD
ABOUT BLUNT AXISYMMETRIC BODIES
AT AN ANGLE OF ATTACK OF 0°**

by Ernest V. Zoby and Randolph A. Graves, Jr.

Langley Research Center

Hampton, Va. 23665

1. Report No. NASA TM X-2843		2. Government Accession No.		3. Recipient's Catalog No.	
4. Title and Subtitle A COMPUTER PROGRAM FOR CALCULATING THE PERFECT GAS INVISCID FLOW FIELD ABOUT BLUNT AXISYMMETRIC BODIES AT AN ANGLE OF ATTACK OF 0°				5. Report Date December 1973	
				6. Performing Organization Code	
7. Author(s) Ernest V. Zoby and Randolph A. Graves, Jr.				8. Performing Organization Report No. L-8944	
9. Performing Organization Name and Address NASA Langley Research Center Hampton, Va. 23665				10. Work Unit No. 502-27-01-01	
				11. Contract or Grant No.	
12. Sponsoring Agency Name and Address National Aeronautics and Space Administration Washington, D.C. 20546				13. Type of Report and Period Covered Technical Memorandum	
				14. Sponsoring Agency Code	
15. Supplementary Notes					
16. Abstract <p>A method for the rapid calculation of the inviscid shock layer about blunt axisymmetric bodies at an angle of attack of 0° has been developed. The procedure is of an inverse nature, that is, a shock wave is assumed and calculations proceed along rays normal to the shock. The solution is iterated until the given body is computed. The flow field solution procedure is programed at the Langley Research Center for the Control Data 6600 computer and requires a core storage of 50000g. The geometries specified in the program are spheres, ellipsoids, paraboloids, and hyperboloids which may have conical afterbodies.</p> <p>The normal momentum equation is replaced with an approximate algebraic expression. This simplification significantly reduces machine computation time. Comparisons of the present results with shock shapes and surface pressure distributions obtained by the more exact methods indicate that the program provides reasonably accurate results for smooth bodies in axisymmetric flow. However, further research is required to establish the proper approximate form of the normal momentum equation for the two-dimensional case.</p>					
17. Key Words (Suggested by Author(s)) Computer program Inviscid flow fields Blunt axisymmetric bodies			18. Distribution Statement Unclassified - Unlimited		
19. Security Classif. (of this report) Unclassified		20. Security Classif. (of this page) Unclassified		21. No. of Pages 56	
				22. Price* Domestic, \$3.50 Foreign, \$6.00	

A COMPUTER PROGRAM FOR CALCULATING THE PERFECT GAS
INVISCID FLOW FIELD ABOUT BLUNT AXISYMMETRIC BODIES
AT AN ANGLE OF ATTACK OF 0°

By Ernest V. Zoby and Randolph A. Graves, Jr.
Langley Research Center

SUMMARY

A method for the rapid calculation of the inviscid shock layer about blunt axisymmetric bodies at an angle of attack of 0° has been developed. The procedure is of an inverse nature, that is, a shock wave is assumed and calculations proceed along rays normal to the shock. The solution is iterated until the given body is computed. The flow field solution procedure is programed at the Langley Research Center for the Control Data 6600 computer and requires a core storage of 50000g. The geometries specified in the program are spheres, ellipsoids, paraboloids, and hyperboloids which may have conical afterbodies.

The normal momentum equation is replaced with an approximate algebraic expression. This simplification significantly reduces machine computation time. Comparisons of the present results with shock shapes and surface pressure distributions obtained by the more exact methods indicate that the program provides reasonably accurate results for smooth bodies in axisymmetric flow. However, further research is required to establish the proper approximate form of the normal momentum equation for the two-dimensional case.

INTRODUCTION

In the past few years, a large effort has been devoted to developing methods for solving the inviscid flow field over blunt bodies traveling at supersonic and hypersonic speeds. Early investigations are documented by Hayes and Probstein (ref. 1), and some of the more recent work is discussed by Grose (ref. 2). Except for the time asymptotic technique, the methods are primarily restricted to the subsonic and slightly supersonic part of the flow field with the downstream supersonic flow being computed by the method of characteristics. A simple approximate but accurate method was developed by Maslen (ref. 3) and was shown to be applicable throughout the subsonic and supersonic regions of the flow field. This method was extended to include nonequilibrium chemistry in reference 2 where it was shown to provide significant reductions in machine storage and computing time over the more exact methods. However, the method as developed in reference 3 is inverse, that is, the shock shape is specified and a resultant flow

field and body are computed. This situation is undesirable since the body shape is usually specified and the flow field and shock shape are to be determined. In addition, the method neglects the normal velocity component and its gradients in the normal momentum equation; these factors account for recompression across the shock layer in the stagnation region. Jackson (ref. 4) devised an iterative scheme to solve the direct problem based on the analysis of reference 3.

In this paper an approximate method has been developed for solving the direct problem of a perfect gas inviscid flow field over blunt bodies at an angle of attack of 0° . The solution incorporates the normal velocity component and the effect of its gradients by replacing the normal momentum equation with an analytic expression developed by Maslen (ref. 5). The present solution uses the basic iterative technique of reference 4 which scales the shock to the specified body in the subsonic and low supersonic region of the flow field. In the downstream supersonic section of the flow field, the shock shape is computed by a "marching" procedure for successive points. The method provides a rapid technique for computing the perfect gas inviscid axisymmetric flow field about blunt bodies such as spheres, paraboloids, ellipsoids, and hyperboloids with an option for conical afterbodies.

This paper presents a discussion of the computational method and results and will serve as a user's manual for the program. A comparison of the results with the results of more exact methods indicates that this method is reasonably accurate. The method is programed at Langley Research Center for the Control Data 6600 computer and requires a core storage of 50000g. A detailed discussion of the program is given in appendix A, and the program listing with a sample case is given in appendix B.

SYMBOLS

<u>Symbol</u>		<u>Program name</u>
a	nondimensional major axis (parallel to flow) of ellipse, a^*/ℓ	ABA
b	nondimensional minor axis (perpendicular to flow) of ellipse, b^*/ℓ	ABB
d	nondimensional diameter, d^*/ℓ	
H_t	nondimensional total enthalpy, $\frac{H_t^*}{U_\infty^{*2}/2}$	HS0
h	nondimensional static enthalpy, $\frac{h^*}{U_\infty^{*2}/2}$	

<u>Symbol</u>		<u>Program name</u>
J	denotes step through shock	
L	body type	L
ℓ	characteristic length (all dimensions nondimensionalized with this term)	
M_s	shock Mach number	MS
M_∞	free-stream Mach number	MINF
N_{it}	iteration number	IT
N_t	number of points across shock layer not including shock point	NT1
N_x	number of rays in subsonic region	NX
n	flow type (0 = Two dimensional; 1 = Axisymmetric)	N
$p(x, y)$	nondimensional pressure through shock layer, $\frac{p^*(x, y)}{(p^*U^2)_\infty}$	
$p(\psi)$	nondimensional pressure through shock layer, $\frac{p^*(\psi)}{(p^*U^2)_\infty}$	PI
p_b	nondimensional body pressure, $\frac{p_b^*}{(\rho^*U^2)_\infty}$	PI(I, NT1)
p_s	nondimensional shock pressure, $\frac{p_s^*}{(\rho^*U^2)_\infty}$	PS
p_{st}	nondimensional body stagnation-point pressure, $\frac{p_{st}}{(p^*U^2)_\infty}$	PST
p_∞^*	free-stream pressure	
ΔR	increment in radius of curvature	DR

<u>Symbol</u>		<u>Program name</u>
R_b	nondimensional body radius of curvature at stagnation point, R_b^*/ℓ	RKB
R_s	nondimensional shock radius of curvature, R_s^*/ℓ	RKSX
R_{st}	nondimensional stagnation-point shock radius of curvature, R_{st}^*/ℓ	RKS1
r	nondimensional cross-sectional radius, r^*/ℓ	RI
r_b	nondimensional cross-sectional body radius, r_b^*/ℓ	RI(I,NT1)
r_c	analytically computed nondimensional cross-sectional body radius, r_c^*/ℓ	RW4C
r_d	nondimensional maximum cross-sectional shock radius, r_d^*/ℓ	REND
r_n	nondimensional nose radius, r_n^*/ℓ	
r_s	nondimensional cross-sectional shock radius, r_s^*/ℓ	RS
S	nondimensional entropy	
U_∞^*	free-stream velocity	
u	nondimensional shock layer velocity in x-direction, u^*/U_∞^*	UI
u_s	nondimensional velocity behind shock in x-direction, u_s^*/U_∞^*	US
v	nondimensional shock layer velocity in y-direction, v^*/U_∞^*	VI
v_s	nondimensional velocity behind shock in y-direction, v_s^*/U_∞^*	VS

<u>Symbol</u>		<u>Program name</u>
x	nondimensional coordinate measured along shock wave from axis of symmetry, x^*/ℓ	XS
x_t	nondimensional total arc length to limiting Mach number, x_t^*/ℓ	XTC
y	nondimensional coordinate normal to shock, y^*/ℓ	YI
y_t	nondimensional value of y from shock to body	YI(I, NT1)
z	nondimensional distance measured along axis of symmetry from shock wave (see fig. 1)	ZI
z_b	nondimensional coordinate measured along axis of symmetry, z_b^*/ℓ	
z_s	nondimensional value of z for shock point, z_s^*/ℓ	ZS
γ	ratio of specific heats	GAM
δ	nondimensional shock stagnation-point standoff distance, δ^*/ℓ	ZST
ϵ	convergence criterion, 1×10^{-4}	EM
$\tilde{\epsilon}$	error	E4(IT)
$\Delta\theta$	increment in shock angle	
θ_b	body angle	THB
θ_s	shock angle	THS
ρ	nondimensional local density, ρ^*/ρ_∞^*	RHI
ρ_s	nondimensional shock density, ρ_s^*/ρ_∞^*	RHOS
ρ_∞^*	free-stream density	

<u>Symbol</u>		<u>Program name</u>
σ_{st}	second derivative of stagnation-point shock radius of curvature	SDERRX
ψ	nondimensional local stream function through shock layer, $\psi^*/\rho_\infty^* U_\infty^{*2} \ell^2$	SY
ψ_s	nondimensional shock stream function, $\psi_s^*/\rho_\infty^* U_\infty^{*2} \ell^2$	SFS

An asterisk * denotes a dimensional quantity. An n as a subscript denotes N_{it} .

RESULTS AND DISCUSSION

The inviscid flow field over blunt bodies is described by the governing equations for an inviscid, nonconducting gas. The equations, for this analysis, are written in an orthogonal curvilinear coordinate system fixed at the axis of symmetry of the shock. (See fig. 1.) Assumptions that the shock layer is thin and that the flow field is axisymmetric are made so that the resulting equations are

Continuity:

$$\left(\frac{\partial (r^n \rho u)}{\partial x} \right)_y + \left(\frac{\partial (r^n \rho v)}{\partial y} \right)_x = 0 \quad (1)$$

x-momentum:

$$u \left(\frac{\partial u}{\partial x} \right)_y + v \left(\frac{\partial u}{\partial y} \right)_x - \frac{uv}{R_s} = - \frac{1}{\rho} \left(\frac{\partial p}{\partial x} \right)_y \quad (2)$$

y-momentum:

$$u \left(\frac{\partial v}{\partial x} \right)_y + v \left(\frac{\partial v}{\partial y} \right)_x + \frac{u^2}{R_s} = - \frac{1}{\rho} \left(\frac{\partial p}{\partial y} \right)_x \quad (3)$$

Entropy:

$$u \left(\frac{\partial S}{\partial x} \right)_y + v \left(\frac{\partial S}{\partial y} \right)_x = 0 \quad (4)$$

Analysis

By following the analysis of reference 3, a Von Mises transformation is introduced so that the independent variables are the distance along the shock x and the stream function ψ . The stream function is defined by

$$\frac{\partial \psi}{\partial y} = -r^n \rho u \quad (5)$$

$$\frac{\partial \psi}{\partial x} = r^n \rho v \quad (6)$$

If these transformations are applied to the governing equations, the continuity equation is automatically satisfied; the y-momentum equation becomes

$$r^n \frac{\partial p}{\partial \psi} = \frac{u}{R_s} + \left(\frac{\partial v}{\partial x} \right)_{\psi} \quad (7)$$

and the entropy equation is

$$\left(\frac{\partial S}{\partial x} \right)_{\psi} = 0 \quad (8)$$

The two momentum equations and the condition that the flow is isoenergetic implies that

$$H_t = h + u^2 + v^2 \quad (9)$$

In addition to equations (7), (8), and (9), the equation of state is

$$h = h(S, p) \quad (10)$$

or

$$\rho = \rho(S, p) \quad (11)$$

For a perfect gas

$$h = \frac{2\gamma}{\gamma - 1} \frac{p}{\rho} \quad (12)$$

and for the condition of isentropic flow along a streamline (eq. (8))

$$\rho = p^{1/\gamma} f(\psi) \quad (13)$$

Note that all the previous parameters were presented in a nondimensional form. Distances are divided by a characteristic length ℓ ; density and velocities by their respective free-stream values; pressure by $(\rho^* U^{*2})_\infty$; the enthalpy by $\frac{1}{2} U_\infty^{*2}$ and the stream function by $(\rho^* U^*)_\infty \ell^{n+1}$.

In the analysis of reference 3, Maslen assumed that $\left(\frac{\partial v}{\partial x}\right)_\psi$ in equation (7) is small and that the streamlines are nearly parallel to the shock, that is, $v \ll u$. Thus, equation (7) can then be approximated as follows with u and r replaced by u_s and r_s , respectively,

$$\frac{\partial p}{\partial \psi} = \frac{u_s}{r_s^n R_s} \quad (14)$$

Integrating from the shock toward the body yields

$$p(\psi) = p_s + \frac{u_s}{r_s^n R_s} (\psi - \psi_s) \quad (15)$$

This analytic equation allows an independent evaluation of the pressure throughout the shock layer and removes many of the usual mathematical problems associated with the subsonic and supersonic regions.

With equation (15) and an equation for the shock shape, a simple procedure can be set up for computing the flow field. The calculations proceed along rays normal to the shock until the body ($\psi = 0$) is reached. Maslen (ref. 3) concluded that the accuracy of such a technique is adequate for general purposes. However, as previously noted, the analysis neglects the normal velocity term in equation (9) and the $\left(\frac{\partial v}{\partial x}\right)_\psi$ term in the normal momentum equation (7). The $\left(\frac{\partial v}{\partial x}\right)_\psi$ term contributes to the recompression in the stagnation region. In this investigation, preliminary calculations verified that the body pressure distributions resulting from equation (15) were approximately 10 to 15 percent lower in the stagnation region than results obtained from more exact methods.

In a more recent investigation, Maslen (ref. 5) considered the $\left(\frac{\partial v}{\partial x}\right)_\psi$ term and by following an analysis similar to reference 3 developed an approximate analytic expression for the pressure. This expression can be written for axisymmetric flow as

$$p(\psi) = p_s + \frac{u_s}{r_s^n R_s} (\psi - \psi_s) + \frac{v_s \tan \theta_s}{r_s^n} \left(\frac{1}{R_s} + \frac{\cos \theta_s}{r_s} \right) \frac{\psi^2 - \psi_s^2}{2\psi_s} \quad (16)$$

Equation (16) is the pressure equation programed in the present computer code.

With the effects of the normal velocity gradients included in equation (16), an approximation to the normal velocity component is necessary. The constant density solution for a sphere (ref. 1) was used as a model, and an approximate expression was developed for this investigation as

$$v(\psi) = v_s \frac{\psi}{\psi_s} \quad (17)$$

Preliminary calculations indicated that equation (17) was satisfactory as an initial guess for the normal velocity profile, but better agreement was obtained with existing results if the normal velocity component is reevaluated during each iteration by

$$v(\psi) = v_s \frac{\left[1 - \frac{y(\psi)}{y_t} \right]^{1.1}}{1 - \frac{y(\psi)}{R_s}} \quad (18)$$

This equation was determined after several trial calculations and comparisons of the data. The rationale for equation (18) is simply the improved agreement of results with published data.

The y-coordinate measured normal to the shock wave is computed with equation (5) written as

$$r^n \frac{\partial y}{\partial \psi} = - \frac{1}{\rho u} \quad (19)$$

and from the flow field geometry (fig. 1)

$$r = r_s - y \cos \theta_s \quad (20)$$

Substituting equation (20) into equation (19) and solving for y gives

$$y = \frac{r_s}{\cos \theta_s} \left[1 - \left(1 - \frac{2 \cos \theta_s}{r_s^2} \int_{\psi}^{\psi_s} \frac{1}{\rho u} d\psi \right)^{1/2} \right] \quad (21)$$

for axisymmetric bodies and

$$y = \int_{\psi}^{\psi_s} \frac{1}{\rho u} d\psi \quad (22)$$

for two-dimensional bodies. In addition, the distance measured along the axis of symmetry from the shock wave is

$$z = z_s + y \sin \theta_s \quad (23)$$

Although the use of equations (16), (17) or (18), and (21) with an equation for the shock shape may produce better agreement with published results than the method in reference 3, the method is still inverse, that is, the computed flow field corresponds to a given shock. The problem of greater engineering interest is the direct problem, that is, computing the shock shape and flow field for a specified body.

Problem Description

The basic steps of an interactive procedure presented by Jackson (ref. 4) are incorporated in this investigation along with the previously discussed flow equations for developing a direct solution of the perfect gas flow field over blunt axisymmetric bodies at an angle of attack of 0° . Note that although the use of the analytic pressure equation (eq. (16)) removes many of the usual mathematical problems associated with the subsonic and supersonic regions, the solution of the direct problem will require separate iterative schemes for the two regions.

In the supersonic region, changes in body shape at a point cannot affect the shock shape or flow field at upstream points; therefore, a step-by-step marching procedure is used. The shock shape and flow field are computed at successive downstream points. However, disturbances, for example, changes in the body shape, in the subsonic region influence the entire region, and this fact requires an iterative procedure for describing the entire subsonic region at once. As discussed by Jackson (ref. 4), the need for computing the entire subsonic—low-supersonic region simultaneously can be illustrated by two flat-faced cylindrical bodies with different body radii. The shock standoff distance and curvature at the stagnation point are different for the two bodies since the scale of the respective subsonic regions is different. Consequently, the shock shapes cannot be calculated by only considering the body shape near the axis of symmetry and computing ahead.

A summary of the iterative techniques is given in the following paragraphs. A more detailed discussion of the iterative techniques is included in the program description in appendix A.

For the subsonic region, the shock shape is represented by a Taylor series in terms of the arc length as

$$R_S(x) = R_{st} + \sigma_{st} \frac{x^2}{2} \quad (24)$$

The shock shape is computed from the axis of symmetry to a point x_t on the shock defined by a shock Mach number of approximately 1.3. For the remainder of this paper, this region is referred to as the subsonic region. The conditions immediately downstream of the shock are determined from the Rankine-Hugoniot relations and the equation

$$d\theta_s = - \frac{dx}{R_S(x)} \quad (25)$$

Along rays perpendicular to the shock, the flow properties are calculated at local values of the stream function by equations (16), (17) or (18), (13), and (9). The calculations continue until the body ($\psi = 0$) is reached. The geometry of each grid point is calculated by equations (21) or (22), (20), and (23). The computed body will probably not agree with the specified body in size or shape. The shock shape and flow field are then scaled to give approximate agreement with the specified body. The difference in the shape of the specified and computed body is defined by an error $\tilde{\epsilon}$. This error is the difference between the radius of the calculated body r_c and the radius of the specified body at the last computed body location in the subsonic region. Depending on the magnitude and sign of the error term $\tilde{\epsilon}$, the σ_{st} value in equation (24) is changed and a new shock shape, a new calculated body, and a new error result. For consistency on successive iterations, the position of x_t is computed so that it corresponds to the same shock angle and Mach number as on the first iteration. The process is repeated until the error is less than some convergence criterion ($\epsilon = 10^{-4}$ for this program).

For this region the specified bodies are given in the program by analytic equations. A sphere, an ellipsoid, a paraboloid, or a hyperboloid may be specified.

If the calculation of the supersonic region is needed, a step-by-step marching-ahead procedure is used to compute the shock shape and flow field. The last converged values of the shock radius of curvature and shock angle in the subsonic region are incremented. The arc length is computed and held constant for the following iterations. By holding the arc length rather than the shock angle constant for iterations in the supersonic region, the shock inflection point resulting from the overexpansion of the flow and the subsequent recompression were found to be easier to compute. The flow properties and the geometry of the grid points are then computed with the same equations as for the subsonic region. The calculated body is compared with the specified body, and an error is computed. A new increment in the shock radius of curvature is determined

and the process is repeated until satisfactory convergence is obtained. The procedure is used to extend the solutions to any downstream distance r_d . As the calculations proceed downstream of the shock inflection point, an option is included for computing sharp cone results (ref. 3) when the shock angle is within a small value (0.001 radian) of the equivalent sharp cone shock angle. This option was included since it was difficult to obtain satisfactory convergence when the shock is nearly straight and the shock radius of curvature is extremely large. In addition to the calculation of the flow field over the analytic body shapes discussed previously, an option is included for computing the supersonic flow fields over conical afterbodies.

Comparison of Results

A comparison of results of existing computational methods for shock shapes and surface pressure distributions with results of the present method is given in figures 2 to 11. These computational methods used for comparison are based on the solution of the full governing inviscid flow equations. Comparisons are presented for a range of Mach numbers and body shapes.

In figures 2 to 8, a comparison of existing shock shape and surface pressure distributions for hemispheres, paraboloids, ellipsoids, and hyperboloids (refs. 6 to 8) with the corresponding results of the present method is shown. The agreement between the present method and the published results is, in general, very good.

In figure 9 the shock shape and pressure distribution for a hemisphere-cylinder at $M_\infty = 7.7$ (ref. 9) are compared with the present results. The present calculations yielded shock standoff distances over the cylindrical section of the body which are approximately 12 percent smaller than those obtained from reference 9. This comparison is similar to that shown in reference 3. The reason for this disagreement may possibly be explained by the assumption in the present analysis of a thin shock layer which is not strictly valid over the cylindrical afterbody. However, the body pressures are predicted very accurately.

In figure 10, the shock shape and pressure distribution over a spherically blunted 30° half-angle cone for $M_\infty = 8$ and $\gamma = 1.4$ computed by the method of reference 10 are compared with the present results. The agreement is very good. At a shock axial location of approximately 2 (see fig. 10(c)), there is an inflection in the shock shape. This shock inflection results from the overexpansion of the flow and subsequent recompression to cone conditions. In figure 11, a similar comparison is made on a spherically blunted 40° half-angle cone at $M_\infty = 38.4$. The flow field computed by the method of reference 10 is in chemical equilibrium. A good match of the shock standoff distance was not obtained with the present method for $\gamma = 1.4$ as would be expected. The shock standoff distances for the present method shown in figure 11 were obtained with

$\gamma = 1.16$. This is the shock stagnation value computed by the method of reference 10. Pressure distributions are shown for $\gamma = 1.16$ and $\gamma = 1.4$. Both agree reasonably well with the results obtained by the method of reference 10.

The results presented previously were for axisymmetric blunt bodies. The present computer code can be applied to two-dimensional bodies. However, initial comparisons of results from reference 11 on two-dimensional cylinders for M_∞ from 4 to 20 and results from the present method indicated some problem areas. Primarily, it was noted that the computed pressures across the shock layer were higher than the body stagnation-point pressure. In developing equation (16), Maslen (ref. 5) assumed the ψ dependence of the recompression term and pointed out that equation (16) was an approximation whose validity could only be established by comparisons with experimental data or exact theoretical analyses. Since the results of the present investigation indicate that the recompression term suggested by Maslen is applicable to axisymmetric bodies but not to two-dimensional bodies, further research is required to establish the proper form for two-dimensional bodies.

From the results presented, it is shown that the present program provides reasonably accurate estimates for quantities such as standoff distances, shock shapes, and surface pressure distributions for axisymmetric flow over smooth bodies.

Existing data for the flow parameters through the shock layer were not as readily available as the shock shape and pressure distribution data. Qualitative comparisons with the results of reference 12 were good except for the profiles near the stagnation line. For example, the tangential velocity is more nonlinear than the results of reference 12 in this region. With the approximations in equations (16) and (17) or (18), such deviations, especially in the stagnation region where the effects of the normal velocity are predominant, are not surprising. In general, the present program provides a reasonably good flow field description. More accurate results could probably be obtained by refining the expression for the normal velocity component (eq. (18)).

CONCLUDING REMARKS

A computer program has been developed for solving the direct problem of a perfect gas inviscid flow field over blunt bodies at an angle of attack of 0° . The geometries specified in the program are spheres, ellipsoids, paraboloids, and hyperboloids which may have conical afterbodies. The calculation procedure is of an inverse nature, that is, a shock wave shape is assumed and calculations proceed along rays normal to the shock, but the shock shape is iterated until the specified body is computed.

The simplifying assumption which significantly decreases machine computation time is that the normal momentum equation is replaced by an explicit analytic expression.

Although these calculations are of an approximate nature, a comparison of the present results with existing shock shapes and surface pressure distributions indicates that the program provides reasonably accurate results.

The option for two-dimensional bodies is included in the program. However, attempts to apply the present approximate form of the normal momentum equation to two-dimensional bodies were not successful, and further research is required to establish the proper form for the two-dimensional case.

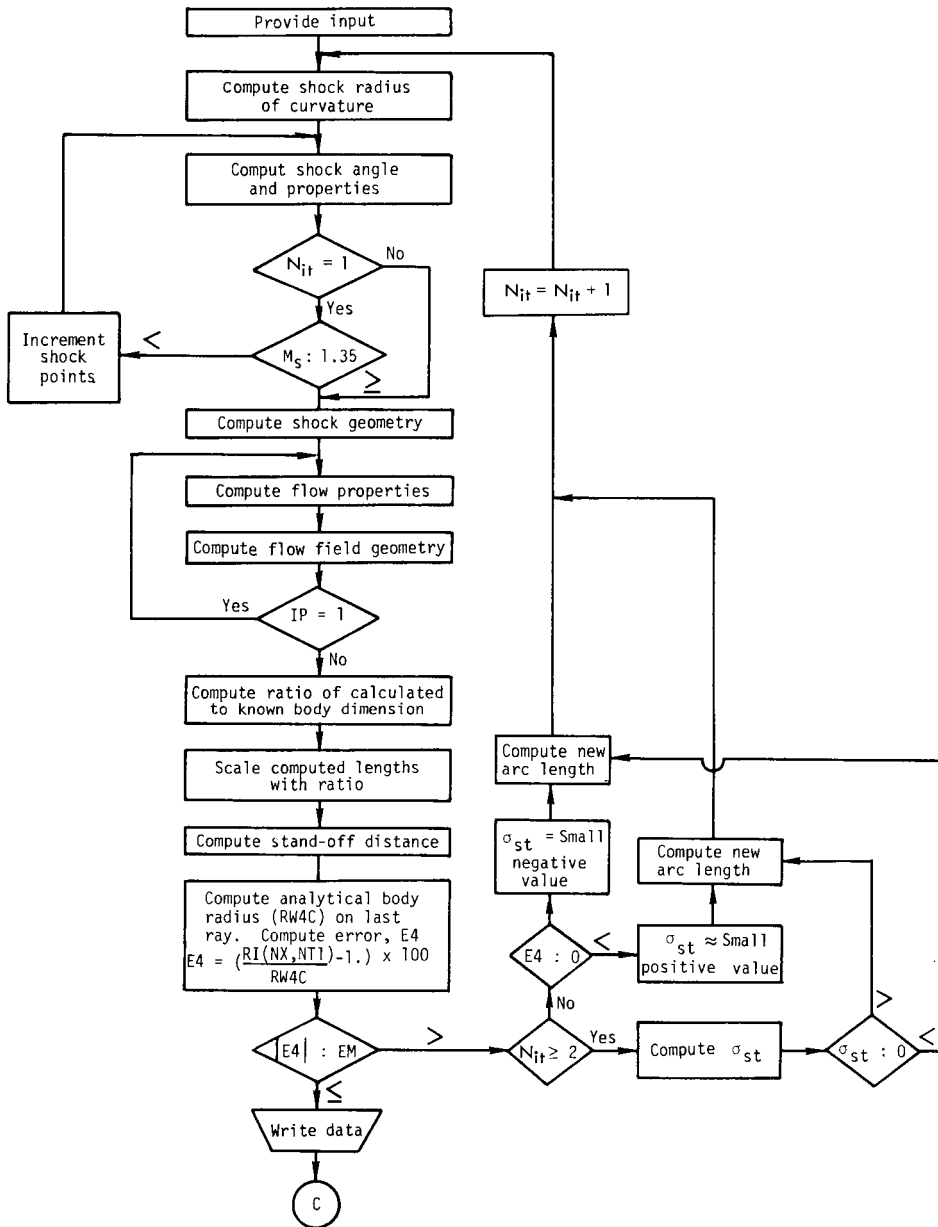
Langley Research Center,
National Aeronautics and Space Administration,
Hampton, Va., August 30, 1973.

APPENDIX A

DETAILED PROGRAM DESCRIPTION

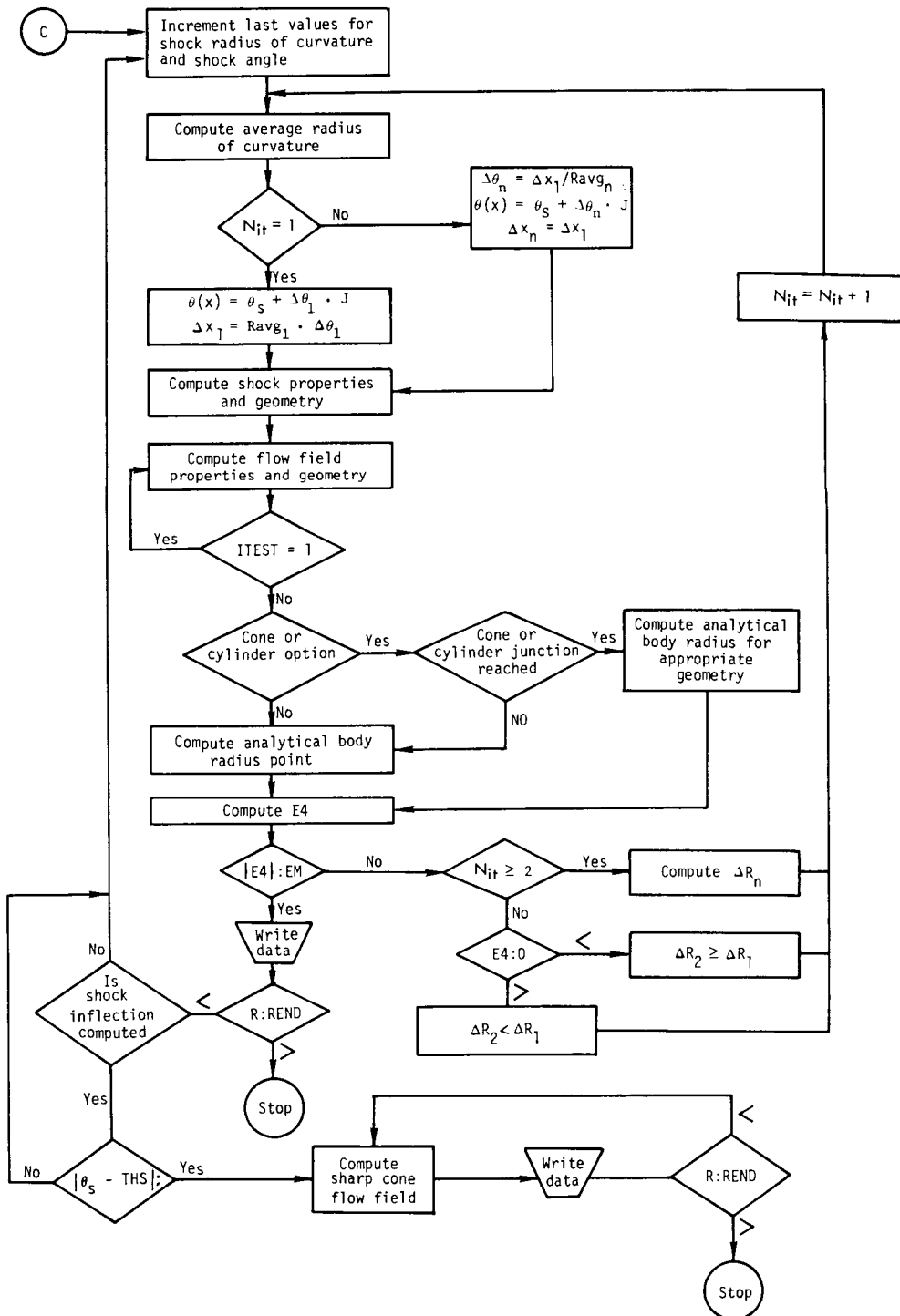
As an aid to a better understanding and a further description of the calculation procedure, flow diagrams are presented with a discussion of the processes.

Flow Diagram for Subsonic Calculation Procedure



APPENDIX A – Continued

Flow Diagram for Supersonic Calculation Procedure



APPENDIX A – Continued

Input

The input for the program is very simple and is primarily restricted to subroutine INITIAL except for the cone half-angle THC required in subroutine SUPER. In INITIAL, the necessary inputs are the free-stream Mach number MINF , the ratio of specific heats GAM , the type of body denoted by L , the type of flow denoted by N , and the radius of curvature of the body RKB . The number of rays is given by N_x or NX and the number of points on the rays is N_t or NT1 . A maximum of seven and a minimum of four rays can be used. Similarly, a maximum of 15 and a minimum of 10 (for consistent results) points along the rays can be used. The stagnation line is considered to be a ray although no calculation is made along this ray. Also, the number of points on a ray do not include the shock point.

Shock Shape

Equation (24) is used to represent the shock-wave shape in the subsonic region. The equation is calculated in the subroutine SADCURV where R_{st} , the shock radius of curvature at the stagnation point, is given as RKS1 and σ_{st} , the second derivative of the radius of curvature at stagnation point, is given as SDERRX(IT) . For the first iteration (IT), RKS1 is assumed to be equal to the body radius of curvature RKB , and SDERRX(1) is 0. The computed value of RKS1 from the procedure is used on further iterations. For the second iteration, SDERRX(2) is assigned an arbitrary small positive or negative value as discussed in the section on iteration procedure in this paper and on subsequent iterations SDERRX(IT) is computed.

With the shock radius of curvature and the arc lengths, the shock angle (THETAS) is computed by equation (25) with a six-point integration routine INT6. The shock angle and the corresponding pressure (PS), velocities (normal (VS) and tangential (US)) and density (RHOS) behind the oblique shock wave are computed at each shock location in subroutine SONIC until the Mach number behind the shock (MS) is equal to approximately 1.3. From experience it was seen that a limiting Mach number near this value produced a smooth transition from the subsonic to supersonic iteration procedure. The angle from the stagnation point to the point on the shock defined by the limiting Mach number is held constant for all iterations so that only the arc length is altered on each successive iteration. The radial (RS) and axial (ZS) locations of each shock point are then determined from the flow field geometry in subroutine SUBGEM. However, for a more rapid procedure, the properties across the shock layer are not computed at each of these shock locations. The arc length to the limiting Mach number is divided into $\text{NX} - 1$ equally spaced regions and NX points on the shock are computed in SUBGEM. The shock geometry and properties at each of these points are then determined from an interpolation scheme in subroutine SUBPROP.

APPENDIX A – Continued

Flow Properties

The simplifying feature of this program is that the normal momentum equation is replaced by an analytic expression from reference 5. This expression is given as equation (16) in this paper and is programed in subroutine PRESLOC.

In references 3 and 4, the normal velocity component (VI) is assumed to be much less than the tangential component (UI) even in a stagnation region and is consequently neglected. An approximation to the normal velocity is given in subroutine PROPLOC. For a first guess, the equation is given as equation (17) in this paper and is reevaluated by equation (18) during each iteration of the shock shape.

The local density is also computed in subroutine PROPLOC. The point on the shock where the local stream function crossed is determined and the density is then simply computed from isentropic relations (eq. (13)). With these flow properties, the tangential velocity is computed from the energy equation.

The local flow properties are computed at points along each ray until the body ($\psi = 0$) is reached. The points are defined by a local stream function which is computed from the stream function at the shock point and equally spaced increments of the stream function along each ray.

Iteration Procedure (Subsonic)

With the flow properties computed, the location (radial, axial, and normal) of each local stream function through the shock layer is computed in subroutine GIP. In order to relate these dimensions to the known body geometry, a scale factor is computed in subroutine BADCURV. The equation for a specified body is passed through the body points computed from the flow field analysis (subroutine GIP), and a relevant length (for instance, the body radius of curvature in the case of a sphere) is computed. The scale factor is the ratio of this relevant length to the known corresponding length for the desired body. All dimensions, shock and body, are then scaled by this ratio in subroutine SCALE. The scaled body points as noted in the subroutine are used with the appropriate analytic equation in subroutine SOSOD to compute the shock stagnation point standoff distance ZST. The value of ZST and the scaled axial length for the last body point in the subsonic region are then used again with the proper analytic body equation to calculate the radial component of this body point in subroutine R4E4. With the scaled and the analytically computed values of this radial location, an error value E4(IT) is also computed in this subroutine. This error value is the percent difference in the two radial calculations. For the second iteration, a small negative value of σ_{st} is assumed if E4(1) is positive, and a small positive value of σ_{st} is assumed if E4(1) is negative. For subsequent iterations, σ_{st} is computed by a Newton-Raphson technique in subroutine SDCORR. A new arc length XTC

APPENDIX A – Continued

to the limiting Mach number is then computed in subroutine CORR1 or CORR2 depending on the sign of σ_{st} . The problem is now iterated until desired convergence is obtained.

Output (Subsonic)

The converged subsonic results are the output of subroutine OUTPUT. The shock and body data are given at six equally spaced shock arc lengths XSP. Note that the complete stagnation-line results are not computed in this program. The flow properties and geometry at each grid point along a ray normal to shock point XSP are also given.

Iteration Procedure (Supersonic)

Although the shock and flow properties are computed in the same manner as in the subsonic region, the iteration procedure is different. No scaling is used and a "marching" technique is employed along the shock. The technique is basically as follows:

(1) A small increment for the last converged values of the shock radius of curvature and shock angle are assumed.

(2) An average radius for the computing interval is calculated and the shock angles are computed within this interval.

(3) The change in arc length is computed and held constant for subsequent iterations.

(4) The shock geometry and properties are computed.

(5) The flow field geometry and properties are computed.

(6) A test is made if a conical option is required, and if it is, another test is made to determine whether the juncture point between the nose and the afterbody is reached. If the juncture point is reached, the body radius point is computed by the routine. When the two tests are negative, the analytic body radius point is computed by the equation used in the subsonic region.

(7) An error value is computed and a new increment for the shock radius of curvature is also computed.

(8) The calculations are iterated until the desired convergence is obtained.

(9) A new step is made along the shock and the same procedures as in steps (2) to (8) are used.

(10) If a shock inflection point is computed, a test is made to determine whether the subsequent computed shock angles are within some small value (0.001 radian) of the equivalent sharp-cone shock angle. If the shock angle is sufficiently close to this value, a sharp-cone solution is used for the following calculations.

(11) Calculations continue until some defined end point on the shock REND is computed.

APPENDIX A – Concluded

Output (Supersonic)

The converged supersonic results are the output of subroutine OUTPUTS at each successive downstream point. The shock and body data are given for this region. Other data, for example, flow properties and geometry of grid points, may be written if desired. The symbols in subroutine OUTPUTS are defined as follows:

ZW	body axial location measured from axis of symmetry of shock
RW	body radial location measured perpendicular to axis of symmetry
YW	body normal location measured perpendicular from shock point
ZS	shock axial location measured from axis of symmetry of shock
RS	shock radial location measured perpendicular to axis of symmetry
PS	pressure at shock
RHOS	density at shock
US	tangential velocity at shock
PW	body pressure
RHOW	body density
UW	body tangential velocity computed normal to ray from shock
MW	Mach number at body
THB	body angle, θ_b , radians

APPENDIX B

PROGRAM LISTING AND SAMPLE OUTPUT

The program listing and sample output follows:

C	PROGRAM DIPGAF	A	1
C	THIS PROGRAM COMPUTES THE PERFECT GAS FLOW FIELD ABOUT A BLUNT TWO	A	2
C	DIMENSIONAL OR AXISYMMETRIC BODY. THE BODY IS KNOWN AND AN INVERSE	A	3
C	TECHNIQUE IS ITERATED UNTIL DESIRED BODY IS FOUND.	A	4
C	THIS MAIN ROUTINE CONTROLS THE SEQUENCE OF CALCULATIONS	A	5
	REAL MINF,MSIN2,MS,MSO,MSI	A	6
	COMMON /BLK1/ GAM,MINF,XINITAL,ZINITAL,RINITAL,THETA IN,SFINITL,L,N	A	7
	1,SDRXINT,RKBN,ABA,ABB,P1,HPA,HPB	A	8
	COMMON /BLK2/ IT,DELX,IBEG,EM,NC,NT1,NX,REND,ND,PST,DR(8),F(200),I	A	9
	1P	A	10
	COMMON /BLK3/ XSP(7),XT,XTC,SCP,RKS,RKSC,RKS1,SDERRX(8),HSO,XS1	A	11
	COMMON /BLK4/ XS(300),RK SX(300),ZS(300),RS(300),SFS(300),THETAS(30	A	12
	10),US(300),PS(300),RHOS(300),MS(300),VS(300)	A	13
	COMMON /BLK5/ RI(7,15),ZI(7,15),YI(7,15),RIC(7,15),ZIC(7,15),YIC(7	A	14
	1,15),RW4C,ZST,E4(8),THB(50)	A	15
	COMMON /BLK6/ SFC(7),RO(7),ZO(7),PO(7),JO(7),THETAO(7),RHOSO(7),MS	A	16
	10(7),RKO(7),DELSY(7),RKOC(7),ROC(7),ZOC(7),VO(7)	A	17
	COMMON /BLK7/ SY(7,15),PI(7,15),RHI(7,15),UI(7,15),MSI(7,15),VI(7,	A	18
	115)	A	19
	CALL INITIAL	A	20
	IT=1+IBEG	A	21
1	CALL SADCURV	A	22
	CALL SONIC	A	23
	CALL SUBGEM	A	24
2	CALL SUBPRCP	A	25
	CALL GIP	A	26
	IF (IP.EQ.2) GO TO 3	A	27
	IP=2	A	28
	GO TO 2	A	29
3	CALL BADCURV	A	30
	CALL SCALE	A	31
	CALL SOSOD	A	32
	CALL R4E4	A	33
	IF (ABS(E4(IT)).LE.EM) GO TO 7	A	34
C		A	35
C	THE SUBSONIC REGION IS COMPUTED IF THIS CRITERIA IS MEET. NOW GO	A	36
C	TO EXIT OR SUPERSONIC REGION.	A	37
C		A	38
	IP=1	A	39
	IF (IT.EQ.1.AND.E4(1).GT.0.0) GO TO 5	A	40
	IF (IT.GT.1) GO TO 8	A	41
	IT=IT+1	A	42
	SDERRX(2)=2.	A	43
4	CALL CORR1	A	44
	GO TO 1	A	45
5	IT=IT+1	A	46
	SDERRX(2)=-2.	A	47
6	CALL CORR2	A	48
	GO TO 1	A	49
7	CALL OUTPUT	A	50
	GO TO 9	A	51
8	CALL SDCORR	A	52
	IF (SDERRX(IT).GT.0.0) GO TO 4	A	53
	GO TO 6	A	54
9	CALL SUPER	A	55
	STOP	A	56
	END	A	57-

APPENDIX B - Continued

C	SUBROUTINE INITIAL	B	1
C		B	2
C	THIS ROUTINE INITIALIZES QUANTITIES PLUS DEFINES CONSTANTS	B	3
C		B	4
	REAL MINF,MSIN2,MS,MSO,MSI	B	5
	COMMON /BLK1/ GAM,MINF,XINITAL,ZINITAL,RINITAL,THETA IN,SFINITL,L,N	B	6
	1,SDRXINT,RKBN,ABA,ABB,P1,HPA,HPB	B	7
	COMMON /BLK2/ IT,DELX,IBEG,EM,NC,NT1,NX,REND,ND,PST,DR(8),F(200),I	B	8
	1P	B	9
	COMMON /BLK3/ XSP(7),XT,XTC,SCP,RKS,RKSC,RKS1,SDERRX(8),HSO,XS1	B	10
	IP=1	B	11
	MINF=10.	B	12
	GAM=1.4	B	13
	XINITAL=0.0	B	14
	ZINITAL=0.0	B	15
	RINITAL=0.0	B	16
	THETA IN=1.5707963268	B	17
	SFINITL=0.0	B	18
	IBEG=0	B	19
	NT1=15	B	20
	REND=1.5	B	21
	NX=7	B	22
	SDRXINT=0.	B	23
	DELX=.015	B	24
	EM=.0001	B	25
C		B	26
C	MINF IS THE FREE STREAM MACH NUMBER;GAM=RATIO OF SPECIFIC HEATS	B	27
C	DELX=INITIAL ARC LENGTH INCRMENT;NT1=NUMBER OF POINTS THRU FLOW	B	28
C	FIELD FOR NUMBER OF RAYS(NX-1)NORMAL TO SHOCK;REND=RADIUS OF SHOCK	B	29
C	WHERE COMPTATIONS STOP;EM=CONVERGENCE CRITERION	B	30
C		B	31
	THH=70.	B	32
	THH=0.01745329252*THH	B	33
	HPB=1.	B	34
	HPA=HPB/TAN(THH)	B	35
	ABA=4.	B	36
	ABB=1.	B	37
	P1=1.0	B	38
	RKBN=1.	B	39
	RKB=P1	B	40
	RKS=RKB	B	41
C		B	42
C	RKB IS RADIUS OF CURVATURE OF BODY. FOR SPHERICAL NOSE,RKB EQUALS	B	43
C	RADIUS OF SPHERE(RKBN). FOR PARABOLA,RKB EQUALS DISTANCE FROM	B	44
C	FOCUS TO DIRECTRIX(P1). FOR ELLIPSE,RKB EQUALS MINOR AXIS SQUARED	B	45
C	RATIOED TO MAJOR AXIS(ABB**2/ABA). FOR HYPERBOLA,RKB EQUALS MINOR	B	46
C	ASYMPTOTE SQUARED RATIOED TO MAJOR ASYMPTOTE(HPB**2/HPA).THH EQUAL	B	47
C	S HALF ANGLE OF HYPERBOLA.NOTE...MAJOR REFERS TO LENGTH PARALLEL	B	48
C	TO ONCOMING STREAM.	B	49
C		B	50
	L=3	B	51
C		B	52
C	IF L EQUALS 1, THE COMPUTED RADIUS OF CURVATURE OF SPHERE WILL BE	B	53
C	SCALING PARAMETER. IF L EQUALS 2,THE COMPUTED MAJOR AXIS OF ELLIPS	B	54
C	E WILL BE SCALING PARAMETER. IF L EQUALS TO 3,THE COMPUTED DISTANC	B	55
C	E FROM FOCUS TO DIRECTRIX OF PARABOLA WILL BE SCALING PARAMETER.	B	56
C	IF L EQUALS 4,THE COMPUTED MAJOR ASYMPTOTE OF HYPERBOLA WILL BE	B	57
C	SCALING PARAMETER.	B	58
C		B	59
	N=1	B	60
C		B	61
C	IF N=1, THE BODY IS AXISYMMETRIC. IF N=0, THE BODY IS 2-D.	B	62
C		B	63
	RETURN	B	64
	END	B	65-

APPENDIX B - Continued

	SUBROUTINE SADCURV	C	1
C		C	2
C	THIS ROUTINE COMPUTES THE SHOCK RADIUS OF CURVATURE AS FUNCTION OF	C	3
C	X. RKS1 IS THE STAGNATION POINT VALUE. RK SX IS VALUE ALONG SHOCK.	C	4
C	XS=SHOCK ARC LENGTH	C	5
C		C	6
	COMMON /BLK1/ GAM,MINF,XINITAL,ZINITAL,RINITAL,THETA IN,SFINITL,L,N	C	7
	1,SDRXINT,RKBN,ABA,ABB,P1,HPA,HPB	C	8
	COMMON /BLK2/ IT,DELX,IBEG,EM,NC,NT1,NX,REND,NU,PST,DR(8),F(200),I	C	9
	1P	C	10
	COMMON /BLK3/ XSP(7),XT,XTC,SCP,RKS,RKSC,RKS1,SDERRX(8),HSC,XS1	C	11
	COMMON /BLK4/ XS(300),RK SX(300),ZS(300),RS(300),SFS(300),THETAS(30	C	12
	10),US(300),PS(300),RHOS(300),MS(300),VS(300)	C	13
	XS(1)=XINITAL	C	14
	IF (IT.GT.1) GO TO 1	C	15
	RK SX(1)=RKS	C	16
	RKS1=RKS	C	17
	SDERRX(1)=SDRXINT	C	18
	NT3=200	C	19
	GO TO 2	C	20
1	RKS1=RKSC	C	21
	RK SX(1)=RKS1	C	22
	NT3=NC	C	23
2	DO 3 I=2,NT3	C	24
	J=I-1	C	25
	XS(I)=XS(J)+DELX	C	26
	RK SX(I)=RKS1+0.5*SDERRX(IT)*XS(I)**2	C	27
3	CONTINUE	C	28
	RETURN	C	29
	END	C	30-

	SUBROUTINE SONIC	D	1
C		D	2
C	THIS ROUTINE COMPUTES SHOCK PROPERTIES IN SUBSONIC REGION UNTIL	D	3
C	LIMITING SHOCK MACH NUMBER IS COMPUTED.	D	4
C	PS=SHOCK PRESSURE,US=SHOCK VELOCITY(TANGENTIAL),VS=SHOCK VELOCITY(D	5
C	NORMAL,RHOS=SHOCK DENSITY,MS=SHOCK MACH NUMBER.	D	6
C		D	7
	REAL MINF,MSIN2,MS,MSQ,PSI	D	8
	COMMON /BLK1/ GAM,MINF,XINITAL,ZINITAL,RINITAL,THETA IN,SFINITL,L,N	D	9
	1,SDRXINT,RKBN,ABA,ABB,P1,HPA,HPB	D	10
	COMMON /BLK2/ IT,DELX,IBEG,EM,NC,NT1,NX,REND,NU,PST,DR(8),F(200),I	D	11
	1P	D	12
	COMMON /BLK3/ XSP(7),XT,XTC,SCP,RKS,RKSC,RKS1,SDERRX(8),HSC,XS1	D	13
	COMMON /BLK4/ XS(300),RK SX(300),ZS(300),RS(300),SFS(300),THETAS(30	D	14

APPENDIX B - Continued

	10),US(300),PS(300),RHOS(300),MS(300),VS(300)	D 15
	BL=((GAM+1.)*MINF)**2	D 16
	DL=4.*GAM*(MINF**2)-2.*(GAM-1.)	D 17
	BLD=(BL/DL)**(GAM/(GAM-1.))	D 18
	THETAS(1)=THETA1N	D 19
	PRAT=2.0/(GAM+1.0)	D 20
	RAT=(GAM-1.0)/(GAM+1.0)	D 21
	GAMM2=1.0/(GAM*MINF**2)	D 22
	IF (IT.GT.1) GO TO 7	D 23
	DO 1 I=1,7	D 24
	F(I)=1.0/RKSX(I)	D 25
1	CONTINUE	D 26
	CALL INT6 (7,DELX,F,B)	D 27
	NN=1	D 28
	MM=7	D 29
	GO TO 4	D 30
2	NN=MM+1	D 31
	MM=MM+2	D 32
	DO 3 I=1,MM	D 33
	F(I)=1.0/RKSX(I)	D 34
3	CONTINUE	D 35
	CALL INT6 (MM,DELX,F,B)	D 36
4	DO 5 I=NN,MM	D 37
	THETAS(I)=THETAS(1)-F(I)	D 38
	US(I)=COS(THETAS(I))	D 39
	US(1)=0.0	D 40
	MSIN2=(MINF*SIN(THETAS(1)))**2	D 41
	PS(I)=(PRAT*(SIN(THETAS(I)))**2)-GAMM2*RAT	D 42
	RHOS(I)=(GAM+1.0)/((GAM-1.0)+(2.0/MSIN2))	D 43
	VS(I)=(1./RHOS(I))*SIN(THETAS(I))	D 44
	AS=SQRT(GAM*PS(I)/RHOS(I))	D 45
	MS(I)=(SQRT((US(I)**2)+VS(I)**2))/AS	D 46
	IF (MS(I).GT.1.3) GO TO 6	D 47
5	CONTINUE	D 48
	GO TO 2	D 49
6	NC=1	D 50
	GO TO 10	D 51
7	DO 8 I=1,NC	D 52
	F(I)=1.0/RKSX(I)	D 53
8	CONTINUE	D 54
	CALL INT6 (NC,DELX,F,B)	D 55
	DO 9 I=1,NC	D 56
	THETAS(I)=THETAS(1)-F(I)	D 57
	US(I)=COS(THETAS(I))	D 58
	US(1)=0.0	D 59
	MSIN2=(MINF*SIN(THETAS(1)))**2	D 60
	PS(I)=(PRAT*(SIN(THETAS(I)))**2)-GAMM2*RAT	D 61
	RHOS(I)=(GAM+1.0)/((GAM-1.0)+(2.0/MSIN2))	D 62
	VS(I)=(1./RHOS(I))*SIN(THETAS(I))	D 63
	AS=SQRT(GAM*PS(I)/RHOS(I))	D 64
	MS(I)=(SQRT((US(I)**2)+VS(I)**2))/AS	D 65
9	CONTINUE	D 66
	PST=PS(1)*BLD	D 67
C		D 68
C	PST IS BODY STAGNATION POINT PRESSURE.	D 69
C		D 70
10	RETURN	D 71
	END	D 72-

APPENDIX B -- Continued

	SUBROUTINE INT6 (NT,DEL,F,B)	E	1
C		E	2
C	ROUTINE IS 6 PCINT INTEGRATION PROCEDURE.	E	3
C		E	4
	DIMENSION X(200), F(200)	E	5
	X(1)=0.0	E	6
	NN2=NT-2	E	7
	NN1=NT-1	E	8
	N=2	E	9
	X(2)=X(1)+((DEL/1440.)*((493.*F(N-1))+ (1337.*F(N))- (618.*F(N+1))+ (E	10
	1302.*F(N+2))- (83.*F(N+3))+ (9.*F(N+4))))	E	11
	N=3	E	12
	X(3)=X(2)+((DEL/129600.)*((-4050.*F(N-2))+ (65430.*F(N-1))+ (75780.*	E	13
	1F(N))- (7020.*F(N+1))- (1170.*F(N+2))+ (630.*F(N+3))))	E	14
	DO 1 N=4,NN2,1	E	15
	X(N)=X(N-1)+((DEL/14400.)*((110.*F(N-3))- (930.*F(N-2))+ (8020.*F(N-	E	16
	11))+ (8020.*F(N))- (930.*F(N+1))+ (110.*F(N+2))))	E	17
1	CONTINUE	E	18
	N=NN1	E	19
	X(N)=X(N-1)+((DEL/14400.)*((-110.*F(N-4))+ (770.*F(N-3))- (2580.*F(N	E	20
	1-2))+ (10220.*F(N-1))+ (6370.*F(N))- (270.*F(N+1))))	E	21
	N=NT	E	22
	X(N)=X(N-1)+((DEL/25920.)*((486.*F(N-5))- (3114.*F(N-4))+ (8676.*F(N	E	23
	1-3))- (14364.*F(N-2))+ (25686.*F(N-1))+ (8550.*F(N))))	E	24
	B=X(NT)	E	25
	DO 2 I=1,NT,1	E	26
	F(I)=X(I)	E	27
2	CONTINUE	E	28
	RETURN	E	29
	END	E	30-

	SUBROUTINE SUBGEM	F	1
C		F	2
C	THIS ROUTINE COMPUTES SHOCK GEOMETRY, STREAM FUNCTION AT SHOCK, AND	F	3
C	DIVIDES SUBSONIC REGION INTO EQUAL SEGMENTS(XSP(I))	F	4
C	RS=RADIAL COMPONENT, ZS=AXIAL COMPONENT, SFS=STREAM FUNCTION AT SHOC	F	5
C	K. ALL LENGTHS ARE MEASURED FROM SHOCK.	F	6
C		F	7
	COMMON /BLK1/ GAM,MINF,XINITAL,ZINITAL,RINITAL,THETA IN,SFINITL,L,N	F	8
	1,SDRXINT,RKBN,ABA,ABB,P1,hPA,hPB	F	9
	COMMON /BLK2/ IT,DELX,IBEG,EM,NC,NT1,NX,REND,ND,PST,DR(8),F(200),I	F	10
	1P	F	11
	COMMON /BLK3/ XSP(7),XT,XTC,SCP,RKS,RKSC,RKS1,SDERRX(8),HSG,XS1	F	12
	COMMON /BLK4/ XS(300),RKX(300),ZS(300),RS(300),SFS(300),THETAS(30	F	13
	10),US(300),PS(300),RHOS(300),MS(300),VS(300)	F	14
	RS(1)=RINITAL	F	15
	ZS(1)=ZINITAL	F	16
	XS(1)=XINITAL	F	17
	SFS(1)=SFINITL	F	18
	DO 1 I=1,NC	F	19
	F(I)=COS(THETAS(I))	F	20
1	CONTINUE	F	21
	CALL INT6 (NC,DELX,F,B)	F	22
	DO 2 I=2,NC	F	23
	ZS(I)=ZS(1)+F(I)	F	24
2	CONTINUE	F	25
	DO 3 I=1,NC	F	26
	F(I)=SIN(THETAS(I))	F	27

APPENDIX B - Continued

3	CONTINUE	F	28
	CALL INT6 (NC,DELX,F,B)	F	29
	DO 4 I=2,NC	F	30
	RS(I)=RS(I)+F(I)	F	31
	SFS(I)=(10.5)**N)*RS(I)**(1+N)	F	32
4	CONTINUE	F	33
	IF (IT.GT.1) GO TO 5	F	34
	XT=XS(NC)	F	35
	XS1=XT	F	36
	DXSP=XT/(NX-1)	F	37
	GO TO 6	F	38
5	XT=XTC	F	39
	DXSP=XT/(NX-1)	F	40
6	DO 7 I=1,NX	F	41
	XSP(I)=(1-1)*DXSP	F	42
7	CONTINUE	F	43
	RETURN	F	44
	END	F	45-

	SUBROUTINE SUBPROP	G	1
C		G	2
C	THIS ROUTINE LOOKS UP THE SHOCK PROPERTIES AND GEOMETRY AT ARC	G	3
C	LENGTHS EQUAL TO XSP(I) AND CALLS ROUTINES PRESLOC AND PROPLCC	G	4
C		G	5
	REAL MINF,MSIN2,MS,MSU,MSI	G	6
	COMMON /BLK1/ GAM,MINF,XINITAL,ZINITAL,RINITAL,THETA IN,SFINITL,L,N	G	7
	1,SDRXINT,RKBN,FEA,ABB,P1,FPA,HPB	G	8
	COMMON /BLK2/ IT,DELX,IBEG,EM,NC,NT1,NX,REND,ND,PST,DR(8),F(200),I	G	9
	1P	G	10
	COMMON /BLK3/ XSF(7),XT,XTC,SCP,RKS,RKSC,RKS1,SDERRX(8),HSO,XS1	G	11
	COMMON /BLK4/ XS(300),RK SX(300),ZS(300),RS(300),SFS(300),THETAS(30	G	12
	10),US(300),PS(300),RHOS(300),MS(300),VS(300)	G	13
	COMMON /BLK6/ SFG(7),RO(7),ZO(7),PC(7),UO(7),THETA O(7),RHOSC(7),MS	G	14
	10(7),RKO(7),DELSY(7),RKOC(7),ROC(7),ZOC(7),VO(7)	G	15
	COMMON /BLK7/ SY(7,15),PI(7,15),RHI(7,15),UI(7,15),MSI(7,15),VI(7,	G	16
	115)	G	17
	DO 1 I=1,NX	G	18
	CALL FTLUP (XSP(I),SFO(I),1,NC,XS,SFS)	G	19
	CALL FTLUP (XSP(I),RO(I),1,NC,XS,RS)	G	20
	CALL FTLUP (XSP(I),ZO(I),1,NC,XS,ZS)	G	21
	CALL FTLUP (XSP(I),PO(I),1,NC,XS,PS)	G	22
	CALL FTLUP (XSP(I),VO(I),1,NC,XS,VS)	G	23
	CALL FTLUP (XSP(I),UO(I),1,NC,XS,US)	G	24
	CALL FTLUP (XSP(I),THETA O(I),1,NC,XS,THETAS)	G	25
	CALL FTLUP (XSP(I),RHOSO(I),1,NC,XS,RHOS)	G	26
	CALL FTLUP (XSP(I),MSU(I),1,NC,XS,MS)	G	27
	CALL FTLUP (XSF(I),RKO(I),1,NC,XS,RK SX)	G	28
1	CONTINUE	G	29
	CALL PRESLOC	G	30
	CALL PROPLCC	G	31
	RETURN	G	32
	END	G	33-

	SUBROUTINE PRESLOC	H	1
C		H	2
C	THIS ROUTINE COMPUTES THE PRESSURE(AT EACH XSP VALUE)ALONG RAYS	H	3
C	NORMAL TO SHOCK. THE PRESSURE EQUATION IS AN APPROXIMATION DEVELOP	H	4
C	ED BY S.H.MASLEN ACCOUNTING FOR THE CENTRIFUGAL AND RECCMPRESSI	H	5
C	EFFECTS.	H	6
C		H	7

APPENDIX B - Continued

	COMMON /BLK1/ GAM,MINF,XINITAL,ZINITAL,RINITAL,THETA IN,SFINITL,L,N	H	8
	1,SDRXINT,RKBN,ABA,ABB,PL,HPA,HPB	H	9
	COMMON /BLK2/ IT,DELX,IBEG,EM,NC,NT1,NX,RENC,ND,PST,DR(8),F(200),I	H	10
	1P	H	11
	COMMON /BLK5/ RI(7,15),ZI(7,15),YI(7,15),RIC(7,15),ZIC(7,15),YIC(7	H	12
	1,15),RW4C,ZST,E4(8),THB(50)	H	13
	COMMON /BLK6/ SFC(7),RO(7),ZO(7),PO(7),UO(7),THETAO(7),RHGSO(7),MS	H	14
	10(7),RKO(7),DELSY(7),RKOC(7),ROC(7),ZOC(7),VO(7)	H	15
	COMMON /BLK7/ SY(7,15),PI(7,15),RHI(7,15),UI(7,15),MSI(7,15),VI(7,	H	16
	115)	H	17
	DO 2 I=2,NX	H	18
	DELSY(I)=SFO(I)/NT1	H	19
	DO 1 J=1,NT1	H	20
	SY(I,J)=SFO(I)-J*DELSY(I)	H	21
	PI(I,J)=PO(I)+(UC(I)/(RKO(I)*(RO(I)**N)))*(SY(I,J)-SFO(I))-((SFO(I	H	22
	1)*VO(I)*TAN(THETAO(I))/(RO(I)**N))*((1./RKO(I))+COS(THETAO(I))/RO	H	23
	2(I)))*((SY(I,J)**2)-SFO(I)**2)/(2.*(SFO(I)**2)))	H	24
1	CONTINUE	H	25
2	CONTINUE	H	26
	RETURN	H	27
	END	H	28-

	SUBROUTINE PROFLOC	I	1
C		I	2
C	THIS ROUTINE COMPUTES THE PROPERTIES (DENSITY=RHI,TANGENTIAL VELOC	I	3
C	ITY=UI,NORMAL VELOCITY=VI,AND MACH NUMBER=MSI) ALONG RAYS NORMAL TO	I	4
C	SHGCK AT XSP VALUES. AN APPROXIMATION TO NORMAL VELOCITY IS USED.	I	5
C		I	6
	REAL MINF,MSIN2,MS,MSO,MSI	I	7
	COMMON /BLK1/ GAM,MINF,XINITAL,ZINITAL,RINITAL,THETA IN,SFINITL,L,N	I	8
	1,SDRXINT,RKBN,ABA,ABB,PL,HPA,HPB	I	9
	COMMON /BLK2/ IT,DELX,IBEG,EM,NC,NT1,NX,RENC,ND,PST,DR(8),F(200),I	I	10
	1P	I	11
	COMMON /BLK3/ XSP(7),XT,XTC,SCP,RKS,RKSC,RKS1,SDERRX(8),HSO,XS1	I	12
	COMMON /BLK4/ XS(300),RK SX(300),ZS(300),RS(300),SFS(300),THETAS(30	I	13
	10),US(300),PS(300),RHOS(300),MS(300),VS(300)	I	14
	COMMON /BLK5/ RI(7,15),ZI(7,15),YI(7,15),RIC(7,15),ZIC(7,15),YIC(7	I	15
	1,15),RW4C,ZST,E4(8),THB(50)	I	16
	COMMON /BLK6/ SFC(7),RO(7),ZO(7),PO(7),UO(7),THETAO(7),RHGSC(7),MS	I	17
	10(7),RKO(7),DELSY(7),RKOC(7),ROC(7),ZOC(7),VO(7)	I	18
	COMMON /BLK7/ SY(7,15),PI(7,15),RHI(7,15),UI(7,15),MSI(7,15),VI(7,	I	19
	115)	I	20
	PRIT=2.0*GAM/(GAM-1.0)	I	21
	HSO=(4.*GAM)/((GAM+1.0)**2)+(((GAM-1.0)/(GAM+1.0))**2)+2./((GAM-1.0)*M	I	22
	1INF**2)	I	23
	DO 3 I=2,NX	I	24
	DO 2 J=1,NT1	I	25
	W=SY(I,J)	I	26
	CALL FTLUP (W,8P,2,NC,SFS,RHCS)	I	27
	CALL FTLUP (W,CP,2,NC,SFS,PS)	I	28
	RHI(I,J)=BP*(PI(I,J)/CP)**(1.0/GAM)	I	29
	PRHE=PI(I,J)/RHI(I,J)	I	30
	IF (IP.EC.2) GO TO 1	I	31
	VI(I,J)=VO(I)*(W/SFC(I))	I	32
	UI(I,J)=SQRT(HSC-PRIT*PRHE-VI(I,J)**2)	I	33
	GO TO 2	I	34
1	VI(I,J)=VO(I)*((1.-(YI(I,J)/YI(I,NT1)))*1.1)*(1./(1.-(YI(I,J)/RKO	I	35
	1(I))))	I	36
	UI(I,J)=SQRT(HSC-PRIT*PRHE-VI(I,J)**2)	I	37
	AE=SQRT(GAM*PI(I,J)/RHI(I,J))	I	38

APPENDIX B - Continued

	MSI(I,J)=(SQRT((UI(I,J)**2)+VI(I,J)**2))/AE	I	39
2	CONTINUE	I	40
3	CONTINUE	I	41
	RETURN	I	42
	END	I	43-

	SUBROUTINE GIP	J	1
C		J	2
C	THIS ROUTINE COMPUTES THE FLOW FIELD COORDINATES. YI=NORMAL COMPONENT; RI=RADIAL COMPONENT; ZI=AXIAL COMPONENT. ALL LENGTHS MEASURED FROM SHOCK.	J	3
C		J	4
C		J	5
C		J	6
	COMMON /BLK1/ GAM,MINF,XINITAL,ZINITAL,RINITAL,THETA IN,SFINITL,L,N	J	7
	1,SDRXINT,RKBN,AEA,ABB,PI,HPA,HPB	J	8
	COMMON /BLK2/ IT,DELX,IBEG,EM,NC,NT1,NX,RENC,ND,PST,DR(8),F(200),I	J	9
	1P	J	10
	COMMON /BLK5/ RI(7,15),ZI(7,15),YI(7,15),RIC(7,15),ZIC(7,15),YIC(7	J	11
	1,15),RW4C,ZST,E4(8),THB(50)	J	12
	COMMON /BLK6/ SFC(7),RO(7),ZO(7),PO(7),UC(7),THETAO(7),RHOSC(7),MS	J	13
	10(7),RKO(7),DELSY(7),RKOC(7),ROC(7),ZOC(7),VO(7)	J	14
	COMMON /BLK7/ SY(7,15),PI(7,15),RHI(7,15),UI(7,15),MSI(7,15),VI(7,	J	15
	115)	J	16
	DO 5 I=2,NX	J	17
	S=-DELSY(I)	J	18
	F(1)=1.0/(RHOSC(I)*UO(I))	J	19
	DO 1 J=1,NT1	J	20
	K=J+1	J	21
	F(K)=1.0/(RHI(I,J)*UI(I,J))	J	22
1	CONTINUE	J	23
	NT2=NT1+1	J	24
	CALL INT6 (NT2,S,F,B)	J	25
	DO 4 J=1,NT1	J	26
	K=1+J	J	27
	IF (N.EQ.0) GO TO 2	J	28
	YI(I,J)=(RO(I)/CCS(THETAO(I)))*(1.0-SQRT(1.0+(2.0*COS(THETAO(I))/R	J	29
	10(I)**2)*F(K)))	J	30
	GO TO 3	J	31
2	YI(I,J)=-F(K)	J	32
3	RI(I,J)=RO(I)-YI(I,J)*CCS(THETAO(I))	J	33
	RP=RO(I)-RI(I,J)	J	34
	SIGMA=1.5707963268-THETAO(I)	J	35
	Z1=RP/(TAN(SIGMA))	J	36
	ZI(I,J)=ZO(I)+Z1	J	37
4	CONTINUE	J	38
5	CONTINUE	J	39
	RETURN	J	40
	END	J	41-

	SUBROUTINE BADCURV	K	1
C		K	2
C	THIS SUBROUTINE COMPUTES THE SCALING PARAMETER FOR THE FLOW BY	K	3
C		K	4
C	RATIDING THE PERTINENT COMPUTED DIMENSION TO THE KNOWN DIMENSION	K	5
	COMMON /BLK1/ GAM,MINF,XINITAL,ZINITAL,RINITAL,THETA IN,SFINITL,L,N	K	6
	1,SDRXINT,RKBN,AEA,ABB,PI,HPA,HPB	K	7

APPENDIX B – Continued

	COMMON /BLK2/ IT,DELX,IBEG,EM,NC,NT1,NX,REND,ND,PST,DR(E),F(200),I	K	8
	1P	K	9
	COMMON /BLK3/ XSP(7),XT,XTC,SCP,RKS,RKSC,RKS1,SDERRX(8),HSD,XS1	K	10
	COMMON /BLK5/ RI(7,15),ZI(7,15),YI(7,15),RIC(7,15),ZIC(7,15),YIC(7	K	11
	1,15),RW4C,ZST,E4(8),THB(50)	K	12
C		K	13
C	IF NX=4 CONTROL POINTS 2 AND 3 MUST BE USED. IF NX=7, CONTROL POINT	K	14
C	S 3 AND 5 RECOMMENDED	K	15
C		K	16
	K=3	K	17
	J=5	K	18
	GO TO (3,2,1,4), L	K	19
1	R2=(RI(K,NT1)**2)-RI(J,NT1)**2	K	20
	Z2=ZI(K,NT1)-ZI(J,NT1)	K	21
	P=0.5*(R2/Z2)	K	22
C		K	23
C	P1 IS THE KNOWN DISTANCE FROM FOCUS TO DIRECTRIX OF PARABOLA.	K	24
C		K	25
	SCP=P/P1	K	26
	GO TO 5	K	27
2	C=(RI(J,NT1)**2)-RI(K,NT1)**2	K	28
	B=(ZI(J,NT1)**2)-ZI(K,NT1)**2	K	29
	A=2.*(ZI(J,NT1)-ZI(K,NT1))	K	30
	E=B/A	K	31
	D=C/A	K	32
	G=E-ZI(K,NT1)	K	33
	C1=(AB8**4)/D**2	K	34
	C2=(2./AB8**2)*G*D+((RI(K,NT1)**2)/(AB8**2))-1.	K	35
	C3=C1*C2	K	36
	C4=(AB8**4)*((G/D)**2)	K	37
	AX=(-C3+SQRT((C3**2)-4.*C4))/2.	K	38
	ABC=SQRT(AX)	K	39
C		K	40
C	ABA IS AXIS OF KNOWN ELLIPSE PARALLEL TO FLOW	K	41
C		K	42
	SCP=ABC/ABA	K	43
	GO TO 5	K	44
3	RB2=(RI(K,NT1)**2)+ZI(K,NT1)**2	K	45
	RB3=(RI(J,NT1)**2)+ZI(J,NT1)**2	K	46
	ZB2=ZI(K,NT1)-ZI(J,NT1)	K	47
	RB23=RB2-RB3	K	48
	ZN=RB23/(2.0*ZB2)	K	49
	RKBC=SQRT(((ZI(K,NT1)-ZN)**2)+RI(K,NT1)**2)	K	50
C		K	51
C	RKBN IS THE KNOWN RADIUS OF CURVATURE OF SPHERE	K	52
C		K	53
	SCP=RKBC/RKBN	K	54
	GO TO 5	K	55
4	B=(RI(K,NT1)**2)-RI(J,NT1)**2	K	56
	C=(ZI(J,NT1)**2)-ZI(K,NT1)**2	K	57
	D=2.*(ZI(K,NT1)-ZI(J,NT1))	K	58
	E=B/D	K	59
	H=C/D	K	60
	G=ZI(K,NT1)+H	K	61
	C1=(HPB**4)/E**2	K	62
	C2=(2./HPB**2)*G*E-((RI(K,NT1)**2)/HPB**2)-1.	K	63
	C3=C1*C2	K	64
	C4=(HPB**4)*((G/E)**2)	K	65
	HX=(-C3+SQRT((C3**2)-4.*C4))/2.	K	66
	HY=SQRT(HX)	K	67
C		K	68
C	HPA IS AXIS OF KNOWN HYPERBOLA PARALLEL TO FLOW	K	69
C		K	70
	SCP=HY/HPA	K	71
5	RETURN	K	72
	END	K	73-

APPENDIX B - Continued

	SUBROUTINE SCALE	L	1
C		L	2
C	THIS ROUTINE MODIFIES ALL LINEAR DIMENSIONS WITH SCALING PARAMETER	L	3
C	(SCP).	L	4
C		L	5
	COMMON /BLK1/ GAM,MINF,XINITAL,ZINITAL,RINITAL,THETA IN,SFINITL,L,N	L	6
	1,SDRXINT,RKBN,ABA,ABB,P1,HPA,HPB	L	7
	COMMON /BLK2/ IT,DELX,IBEG,EM,NC,NT1,NX,RENC,ND,PST,DR(8),F(200),I	L	8
	1P	L	9
	COMMON /BLK3/ XSP(7),XT,XTC,SCP,RKS,RKSC,RKS1,SDERRX(8),HSO,XS1	L	10
	COMMON /BLK4/ XS(300),RK SX(300),ZS(300),RS(300),SFS(300),THETAS(30	L	11
	10),US(300),PS(300),RHOS(300),MS(300),VS(300)	L	12
	COMMON /BLK5/ RI(7,15),ZI(7,15),YI(7,15),RIC(7,15),ZIC(7,15),YIC(7	L	13
	1,15),RW4C,ZST,E4(8),THB(50)	L	14
	COMMON /BLK6/ SFC(7),RO(7),ZC(7),PC(7),UO(7),THETAQ(7),RHOSO(7),MS	L	15
	1D(7),RKO(7),DELSY(7),RKOC(7),ROC(7),ZOC(7),VO(7)	L	16
	IF (L.EQ.2.OR.L.EQ.4) GO TO 1	L	17
	SCP=1.0/SCP	L	18
1	RKSC=RKS1*SCP	L	19
	DO 2 I=2,NX	L	20
	RIC(I,NT1)=RI(I,NT1)*SCP	L	21
	ZIC(I,NT1)=ZI(I,NT1)*SCP	L	22
	YIC(I,NT1)=YI(I,NT1)*SCP	L	23
	ZOC(I)=ZC(I)*SCP	L	24
	ROC(I)=RO(I)*SCP	L	25
	RKOC(I)=RKOC(I)*SCP	L	26
2	CONTINUE	L	27
	DO 3 I=1,NC	L	28
	XS(I)=XS(I)*SCP	L	29
	RS(I)=RS(I)*SCP	L	30
	ZS(I)=ZS(I)*SCP	L	31
	RK SX(I)=RK SX(I)*SCP	L	32
3	CONTINUE	L	33
	RETURN	L	34
	END	L	35-

	SUBROUTINE SOSCD	M	1
C		M	2
C	THIS ROUTINE COMPUTES THE STAGNATION-POINT SHOCK STAND-OFF	M	3
C	DISTANCE (ZST) AND THE RESPECTIVE BODY ANGLES (THB). THB IS ANGLE OF	M	4
C	INCLINATION OF BODY SURFACE WITH LONGITUDINAL AXIS.	M	5
C		M	6
	COMMON /BLK1/ GAM,MINF,XINITAL,ZINITAL,RINITAL,THETA IN,SFINITL,L,N	M	7
	1,SDRXINT,RKBN,ABA,ABB,P1,HPA,HPB	M	8
	COMMON /BLK2/ IT,DELX,IBEG,EM,NC,NT1,NX,RENC,ND,PST,DR(8),F(200),I	M	9
	1P	M	10
	COMMON /BLK5/ RI(7,15),ZI(7,15),YI(7,15),RIC(7,15),ZIC(7,15),YIC(7	M	11
	1,15),RW4C,ZST,E4(8),THB(50)	M	12
C		M	13
C	IF NX=4,CONTROL POINT 2 MUST BE USED. IF NX=7,CONTROL POINT 3 RECC-	M	14
C	MEDED.	M	15
C		M	16
	K=3	M	17
	GO TO (3,2,1,4), L	M	18
1	B1=ZIC(K,NT1)	M	19
	B2=-((RIC(K,NT1)**2)/(2.*P1))	M	20
	GO TO 5	M	21
2	B1=ZIC(K,NT1)-ABA	M	22
	B2=SQRT((ABA**2)-((ABA/ABB)**2)*RIC(K,NT1)**2)	M	23
	GO TO 5	M	24
3	B1=ZIC(K,NT1)-RKBN	M	25

APPENDIX B - Continued

	B2=SQRT((RKBN**2)-RIC(K,NT1)**2)	M	26
	GO TO 5	M	27
4	B1=ZIC(K,NT1)+HPA	M	28
	B2=-SQRT((HPA**2)+((HPA/HPB)**2)*RIC(K,NT1)**2)	M	29
5	ZST=B1+B2	M	30
	LM=NX-1	M	31
	DO 10 I=1,LM	M	32
	J=I+1	M	33
	GO TO (6,7,8,9), L	M	34
6	THB(I)=ATAN((RKBN-(ZIC(J,NT1)-ZST))/RIC(J,NT1))	M	35
	GO TO 10	M	36
7	THB(I)=ATAN(((ABB/ABA)**2)*(ABA-ZIC(J,NT1)+ZST)/RIC(J,NT1))	M	37
	GO TO 10	M	38
8	THB(I)=ATAN(P1/RIC(J,NT1))	M	39
	GO TO 10	M	40
9	THB(I)=ATAN(((HPB/HPA)**2)*(HPA+ZIC(J,NT1)-ZST)/RIC(J,NT1))	M	41
10	CONTINUE	M	42
	RETURN	M	43
	END	M	44-

	SUBROUTINE R4E4	N	1
C		N	2
C	THIS ROUTINE COMPUTES THE ANALYTICAL BODY RADIUS AT LAST BODY POINT	N	3
C	T(NX,NT1) WITH COMPUTED ZIC(NX,NT1) AND ZST.	N	4
C	ALSO ERROR BETWEEN COMPUTED BODY(RIC(NX,NT1)) AND ANALYTICAL	N	5
C	BODY(RW4C) IS DETERMINED.	N	6
C		N	7
	COMMON /BLK1/ GAM,MINF,XINITAL,ZINITAL,RINITAL,THETAIN,SFINITL,L,N	N	8
	1,SDRXINT,RKBN,ABA,ABB,P1,HPA,HPB	N	9
	COMMON /BLK2/ IT,DELX,IBEG,EM,NC,NT1,NX,REND,ND,PST,DR(8),F(200),I	N	10
	1P	N	11
	COMMON /BLK5/ RI(7,15),ZI(7,15),YI(7,15),RIC(7,15),ZIC(7,15),YIC(7	N	12
	1,15),RW4C,ZST,E4(8),THB(50)	N	13
	GO TO (3,2,1,4), L	N	14
1	RW4C=SQRT(2.*P1*(ZIC(NX,NT1)-ZST))	N	15
	GO TO 5	N	16
2	B3=SQRT((ABA**2)-((ABA+ZST)-ZIC(NX,NT1))**2)	N	17
	RW4C=(ABB/ABA)*B3	N	18
	GO TO 5	N	19
3	B3=(ZIC(NX,NT1)-(RKBN+ZST))**2	N	20
	RW4C=SQRT((RKBN**2)-B3)	N	21
	GO TO 5	N	22
4	B3=SQRT(((ZIC(NX,NT1)+HPA-ZST)**2)-HPA**2)	N	23
	RW4C=(HPB/HPA)*B3	N	24
5	E4(IT)=((RIC(NX,NT1)/RW4C)-1.)*100.	N	25
	RETURN	N	26
	END	N	27-

	SUBROUTINE CORR1	O	1
C		O	2
C	THIS ROUTINE IS USED TO CORRECT THE LENGTH ALONG SHOCK TO SONIC	O	3
C	REGION(XTC) IF THE VALUE OF SDERRX IS POSITIVE FOR THE PARTICULAR	C	4
C	ITERATION(IT).	O	5
C		O	6
	COMMON /BLK2/ IT,DELX,IBEG,EM,NC,NT1,NX,REND,ND,PST,DR(8),F(200),I	O	7

APPENDIX B - Continued

1P		O	8
COMMON /BLK3/ XSP(7),XT,XTC,SCP,RKS,RKSC,RKS1,SDERRX(8),HSC,XS1		O	9
SDERRX2=0.5*SDERRX(1T)		O	10
RIG=SDERRX2/RKSC		O	11
SRIG=SQRT(RIG)		O	12
XRK=(XS1*RKSC)/RKS		O	13
XTC=SQRT(1.0/RIG)*TAN(SRIG*XRK)		O	14
DELX=XTC/(NC-1)		O	15
RETURN		O	16
END		O	17-

	SUBROUTINE CORR2	P	1
C		P	2
C	THIS ROUTINE IS USED TO CORRECT THE LENGTH TO THE SONIC POINT(XTC)	P	3
C	IF SDERRX IS NEGATIVE FOR THE ITERATION(1T).	P	4
C		P	5
	COMMON /BLK2/ 1T,DELX,IBEG,EM,NC,NT1,NX,RENC,ND,PST,DR(8),F(200),I	P	6
1P		P	7
	COMMON /BLK3/ XSP(7),XT,XTC,SCP,RKS,RKSC,RKS1,SDERRX(8),HSC,XS1	P	8
	SDERRX2=0.5*SDERRX(1T)	P	9
	SRKSS=SQRT(ABS(SCERRX2)/RKSC)	P	10
	SRKSD=SQRT(RKSC/ABS(SDERRX2))	P	11
	XRK=(XS1*RKSC)/RKS	P	12
	EXP1=EXP(2.0*SRKSS*XRK)	P	13
	EXPN=EXP1-1.0	P	14
	EXPD=EXP1+1.0	P	15
	EXPQ=EXPN/EXPD	P	16
	XTC=SRKSD*EXPQ	P	17
	DELX=XTC/(NC-1)	P	18
	RETURN	P	19
	END	P	20-

	SUBROUTINE SOCORR	Q	1
C		Q	2
C	THIS ROUTINE COMPUTES SDERRX IF IT IS GREATER THAN 2	C	3
C		Q	4
	COMMON /BLK2/ 1T,DELX,IBEG,EM,NC,NT1,NX,RENC,ND,PST,DR(8),F(200),I	Q	5
1P		Q	6
	COMMON /BLK3/ XSP(7),XT,XTC,SCP,RKS,RKSC,RKS1,SDERRX(8),HSC,XS1	Q	7
	COMMON /BLK5/ RI(7,15),ZI(7,15),YI(7,15),RIC(7,15),ZIC(7,15),YIC(7	Q	8
	1,15),RW4C,ZST,E4(8),THB(50)	Q	9
	1T=1T+1	Q	10
	IF (1T.EQ.9) SDERRX(1)=SDERRX(7)	Q	11
	IF (1T.EQ.9) SDERRX(2)=SDERRX(8)	C	12
	IF (1T.EQ.9) E4(1)=E4(7)	Q	13
	IF (1T.EQ.9) E4(2)=E4(8)	Q	14
	IF (1T.EQ.9) 1T=3	Q	15
	SDERRX(1T)=SDERRX(1T-1)-E4(1T-1)*(SDERRX(1T-1)-SDERRX(1T-2))/(E4(1	Q	16
	1T-1)-E4(1T-2))	Q	17
	RETURN	Q	18
	END	Q	19-

APPENDIX B – Continued

	SUBROUTINE OUTPUT	R	1
	REAL MINF,MSIN2,MS,MSO,MSI	R	2
	COMMON /BLK2/ IT,DELX,IBEG,EM,NC,NT1,NX,REND,ND,PST,DR(8),F(200),I	R	3
	1P	R	4
	COMMON /BLK3/ XSP(7),XT,XTC,SCP,RKS,RKSC,RKS1,SDERRX(8),HSC,XS1	R	5
	COMMON /BLK5/ RI(7,15),ZI(7,15),YI(7,15),RIC(7,15),ZIC(7,15),YIC(7	R	6
	1,15),RW4C,ZST,E4(8),THB(50)	R	7
	COMMON /BLK6/ SFC(7),RO(7),ZO(7),PO(7),UO(7),THETAO(7),RHOSO(7),MS	R	8
	10(7),RKO(7),DELSY(7),RKOC(7),ROC(7),ZOC(7),VO(7)	R	9
	COMMON /BLK7/ SY(7,15),PI(7,15),RHI(7,15),UI(7,15),MSI(7,15),VI(7,	R	10
	115)	R	11
	WRITE (6,7) RKSC,ZST	R	12
	WRITE (6,8) PST	R	13
	WRITE (6,9)	R	14
	DO 1 I=2,NX	R	15
	WRITE (6,10) XSP(I),ZOC(I),ROC(I),ZIC(I,NT1),RIC(I,NT1),YIC(I,NT1)	R	16
	1,RKOC(I)	R	17
1	CONTINUE	R	18
	WRITE (6,11)	R	19
	DO 2 I=2,NX	R	20
	J=I-1	R	21
	WRITE (6,10) MSI(I,NT1),PO(I),UO(I),VO(I),RHOSO(I),MSO(I),THB(J)	R	22
2	CONTINUE	R	23
	DO 6 I=2,NX	R	24
	WRITE (6,15) XSF(I)	R	25
	IF (1.GT.2) GO TO 3	R	26
	WRITE (6,12)	R	27
3	DO 4 J=1,NT1	R	28
	WRITE (6,16) PI(I,J),RHI(I,J),UI(I,J),VI(I,J),MSI(I,J),SY(I,J)	R	29
4	CONTINUE	R	30
	WRITE (6,13)	R	31
	DO 5 J=1,NT1	R	32
	WRITE (6,14) YI(I,J),ZI(I,J),RI(I,J)	R	33
5	CONTINUE	R	34
6	CONTINUE	R	35
	RETURN	R	36
C		R	37
7	FORMAT (/3X,22H STAG PT SHK RAD CUR =,E11.4,5X,28H STAG PT STAND O	R	38
	1FF DIST =,E11.4)	R	39
8	FORMAT (3X,19HBCDY STAG PT PRESS=,E11.4)	R	40
9	FORMAT (/74X,10HARC LENGTH,3X,15HSHOCK AXIAL LOC,3X,16HSHOCK RADIA	R	41
	1L LOC,3X,14HBCDY AXIAL LOC,3X,15HBCDY RADIAL LOC,3X,15HBCDY NORMAL	R	42
	2 LOC,3X,20HSHOCK RADIALS OF CURV)	R	43
10	FORMAT (3XE11.4,5XE11.4,7XE11.4,7XE11.4,6XE11.4,7XE11.4,8XE11.4)	R	44
11	FORMAT (/74X,10HMACH NO WL,3X,15HSHOCK PRESSURE,3X,16HTAN SHK VELO	R	45
	1CITY,3X,16HNOR SHK VELOCITY,3X,14HSHOCK DENSITY,3X,15HSHOCK MACH N	R	46
	2UMB,6X,10HBCDY ANGLE)	R	47
12	FORMAT (/73X,14HFIELD PRESSURE,4X,13HFIELD DENSITY,4X,2CHFIELD VEL	R	48
	LOCITY(TANG),4X,20HFIELD VELOCITY(NORM),4X,13HFIELD MACH NC,4X,15HF	R	49
	2IELD STRM FUNC)	R	50
13	FORMAT (/73X,55HFIELD NCRMAL LOC FIELD AXIAL LOC FIELD RADIA	R	51
	1L LOC)	R	52
14	FORMAT (5XE11.4,6XE11.4,8XE11.4)	R	53
15	FORMAT (/73X,5H XSP=,E11.4)	R	54
16	FORMAT (5XE11.4,6XE11.4,7XE11.4,14XE11.4,10XE11.4,7XE11.4)	R	55
	END	R	56-

APPENDIX B - Continued

	SUBROUTINE SUPER	S	1
C		S	2
C	THIS ROUTINE COMPUTES THE SUPERSONIC FLOW FIELD.	S	3
C		S	4
	REAL MINF,MSIN2,MS,MSO,MSI	S	5
	COMMON /BLK1/ GAM,MINF,XINITAL,ZINITAL,RINITAL,THETA IN,SFINITL,L,N	S	6
	1,SORXINT,RKBN,ABA,ABB,P1,HPA,HPB	S	7
	COMMON /BLK2/ IT,DELX,IBEG,EM,NC,NT1,NX,REND,ND,PST,DR(8),F(200),I	S	8
	1P	S	9
	COMMON /BLK3/ XSF(7),XT,XTC,SCP,RKS,RKSC,RKS1,SUERRX(8),HSO,XS1	S	10
	COMMON /BLK4/ XS(300),RKXS(300),ZS(300),RS(300),SFS(300),THETAS(30	S	11
	10),US(300),PS(300),RHOS(300),MS(300),VS(300)	S	12
	COMMON /BLK5/ RI(7,15),ZI(7,15),YI(7,15),RIC(7,15),ZIC(7,15),YIC(7	S	13
	1,15),RW4C,ZST,E4(8),THB(50)	S	14
	COMMON /BLK6/ SFG(7),RO(7),ZO(7),PO(7),UC(7),THETAQ(7),RHOSC(7),MS	S	15
	10(7),RKO(7),DELSY(7),RKOC(7),RUC(7),ZOC(7),VO(7)	S	16
	COMMON /BLK7/ SY(7,15),PI(7,15),RHI(7,15),UI(7,15),MSI(7,15),VI(7,	S	17
	115)	S	18
	DIMENSION RB(20), ZB(20)	S	19
	IOPT=0	S	20
	THC=0.	S	21
	THC=0.01745329252*THC	S	22
C		S	23
C	IF IOPT=0,ANALYTIC CALCULATION CONTINUES THROUGH SUPERSONIC REGION	S	24
C	IF IOPT=1,A CONE JUNCTURE WILL BE MATCHED TO ANALYTIC SHAPE. THC=	S	25
C	BLUNT CONE HALF ANGLE.IF THC=0 AND IOPT=1,A CYLINDER WILL BE MATCH	S	26
C	ED TO ANALYTIC SHAPE.	S	27
C		S	28
	DETHB=.0	S	29
	ITEST=1	S	30
	NH=0	S	31
	NHC=0	S	32
	NHH=0	S	33
	THS1=0.	S	34
	ISUM=NX-1	S	35
	DO 1 J=1,ISUM	S	36
	I=J+1	S	37
	RB(J)=RIC(I,NT1)	S	38
	ZB(J)=ZIC(I,NT1)	S	39
1	CONTINUE	S	40
	ICOUNT=0	S	41
	RHS=0.	S	42
	R1=0.0	S	43
	THSC=ASIN(SQRT(((1./MINF**2)+((GAM+1.)/2.)*SIN(THC)**2)))	S	44
C		S	45
C	THIS EQUATION COMPUTES SHARP CONE SHOCK ANGLE.	S	46
C		S	47
	NP=0	S	48
	PRIT=2.0*GAM/(GAM-1.0)	S	49
	GAMM2=1.0/(GAM*MINF**2)	S	50
	RAT=(GAM-1.0)/(GAM+1.0)	S	51
	PRAT=2.0/(GAM+1.0)	S	52
	DR(1)=.1	S	53
	IT=1	S	54
	DETH=(THETAS(NC)-THETAS(NC-1))/1.5	S	55
	IZ=0	S	56
2	ND=NC+7	S	57
	ID=0	S	58
3	RKSX(ND)=RKSX(NC)+CR(IT)	S	59
C		S	60
C	THE SHOCK RADIUS OF CURVATURE IS COMPUTED	S	61
C		S	62
	RKC2=0.5*(RKSX(ND)+RKSX(NC))	S	63
	NA=NC+1	S	64
	IF (IT.GT.1) THETAS(ND)=THETAS(NC)+(RKXS/RKC2)	S	65
	IF (IT.GT.1) DETH=(THETAS(ND)-THETAS(NC))/7.	S	66

APPENDIX B - Continued

	DO 4 I=1,8	S 67
	F(I)=-RKC2	S 68
4	CONTINUE	S 69
	CALL INT6 (8,DETH,F,8)	S 70
C		S 71
C	THE FOLLOWING DO LOOP COMPUTES SHOCK PROPERTIES	S 72
C		S 73
	DO 5 I=NA,ND	S 74
	THETAS(I)=THETAS(I-1)+DETH	S 75
	M=I-NC+1	S 76
	XS(I)=XS(NC)+F(M)	S 77
	IF (IZ.EQ.1.AND.RKXS(NC).GT.0.) XS(I)=XS(NC)-F(M)	S 78
	US(I)=COS(THETAS(I))	S 79
	MSIN2=(MINF*SIN(THETAS(I)))**2	S 80
	PS(I)=(PRAT*SIN(THETAS(I)))**2-GAMM2*PRAT	S 81
	RHOS(I)=(GAM+1.0)/((GAM-1.0)+(2.0/MSIN2))	S 82
	VS(I)=(1.0/RHOS(I))*SIN(THETAS(I))	S 83
	AS=SQRT(GAM*PS(I)/RHOS(I))	S 84
	MS(I)=(SQRT((US(I)**2)+VS(I)**2))/AS	S 85
5	CONTINUE	S 86
	IF (IT.EQ.1) RKXS=RKC2*(THETAS(ND)-THETAS(NC))	S 87
C		S 88
C	THE FOLLOWING ROUTINE COMPUTES THE SHOCK GEOMETRY.	S 89
C		S 90
	DELX=(XS(NC)-XS(NC))/7.	S 91
	DO 6 I=NC,ND	S 92
	M=I-NC+1	S 93
	F(M)=COS(THETAS(I))	S 94
6	CONTINUE	S 95
	CALL INT6 (8,DELX,F,8)	S 96
	DO 7 I=NA,ND	S 97
	M=I-NC+1	S 98
	ZS(I)=ZS(NC)+F(M)	S 99
7	CONTINUE	S 100
	DO 8 I=NC,ND	S 101
	M=I-NC+1	S 102
	F(M)=SIN(THETAS(I))	S 103
8	CONTINUE	S 104
	CALL INT6 (8,DELX,F,8)	S 105
	DO 9 I=NA,ND	S 106
	M=I-NC+1	S 107
	RS(I)=RS(NC)+F(M)	S 108
	SFS(I)=((0.5**N)*RS(I)**(1+N))	S 109
9	CONTINUE	S 110
C		S 111
C	THE FOLLOWING ROUTINE COMPUTES THE PROPERTIES ALONG A RAY	S 112
C		S 113
	S=SFS(ND)/NT1	S 114
	ITEST=1	S 115
10	DO 12 J=1,NT1	S 116
	IF (ITEST.EQ.2) GO TO 11	S 117
	SY(4,J)=SFS(ND)-J*S	S 118
	PI(4,J)=PS(ND)+(US(ND)/(RKXS(ND)*(RS(ND)**N)))*(SY(4,J)-SFS(ND))-	S 119
	1(SFS(ND)*VS(ND)*TAN(THETAS(ND))/(RS(ND)**N))*((1./RKXS(ND))+COS(TH	S 120
	2ETAS(ND))/RS(ND)))*(((SY(4,J)**2)-(SFS(ND)**2))/(2.*(SFS(ND)**2)))	S 121
	W=SY(4,J)	S 122
	CALL FTLUP (W,BP,1,NC,SFS,RHOS)	S 123
	CALL FTLUP (W,CP,1,NC,SFS,PS)	S 124
	RHI(4,J)=BP*(PI(4,J)/CP)**(1.0/GAM)	S 125
	PRHE=PI(4,J)/RHI(4,J)	S 126
	VI(4,J)=VS(ND)*(W/SFS(ND))	S 127
	UI(4,J)=SQRT(HSC-PRIT*PRHE-VI(4,J)**2)	S 128
	GO TO 12	S 129
11	W=SY(4,J)	S 130
	VI(4,J)=VS(ND)*((1.-(YI(4,J)/YI(4,NT1)))*(1./(1.-(YI(4,J)/RKXS(ND	S 131
	1))))	S 132

APPENDIX B - Continued

	PRHE=PI(4,J)/RHI(4,J)	S 133
	UI(4,J)=SQRT(HSO-PRIT*PRHE-VI(4,J)**2)	S 134
	AE=SQRT(GAM*PRHE)	S 135
	MSI(4,J)=(SQRT((UI(4,J)**2)+VI(4,J)**2))/AE	S 136
12	CONTINUE	S 137
C		S 138
C	THE FOLLOWING STATEMENTS COMPUTE THE FLOW FIELD GEOMETRY.	S 139
C		S 140
	F(1)=1.0/(RFUS(ND)*US(ND))	S 141
	DO 13 J=1,NT1	S 142
	K=1+J	S 143
	F(K)=1.0/(RHI(4,J)*UI(4,J))	S 144
13	CONTINUE	S 145
	NT2=NT1+1	S 146
	CALL INT6 (NT2,S,F,B)	S 147
	DO 16 J=1,NT1	S 148
	K=1+J	S 149
	IF (N.EQ.0) GO TO 14	S 150
	YI(4,J)=(RS(ND)/COS(THETAS(ND)))*(1.0-SQRT(1.0-(2.0*COS(THETAS(ND)	S 151
	1)/RS(ND)**2)*F(K)))	S 152
	GO TO 15	S 153
14	YI(4,J)=F(K)	S 154
15	RI(4,J)=RS(ND)-YI(4,J)*CCS(THETAS(ND))	S 155
	SIGMA=THETA IN-THETAS(ND)	S 156
	RP=RS(ND)-RI(4,J)	S 157
	Z1=RP/(TAN(SIGMA))	S 158
	ZI(4,J)=ZS(ND)+Z1	S 159
16	CONTINUE	S 160
	IF (ITEST.EQ.2) GO TO 17	S 161
	YS=YI(4,NT1)	S 162
	ITEST=2	S 163
	GO TO 10	S 164
C		S 165
C	THE FOLLOWING STATEMENTS SCALE THE FLOW FIELD	S 166
C		S 167
17	IF (ABS(YS-YI(4,NT1)).LE..00001) GO TO 18	S 168
	YS=YI(4,NT1)	S 169
	GO TO 10	S 170
18	RIC(4,NT1)=RI(4,NT1)	S 171
	ZIC(4,NT1)=ZI(4,NT1)	S 172
	YIC(4,NT1)=YI(4,NT1)	S 173
	ZOC(4)=ZS(ND)	S 174
	ROC(4)=RS(ND)	S 175
	RKOC(4)=RKC2	S 176
C		S 177
C	THE FOLLOWING STATEMENTS COMPARE THE COMPUTED AND ANALYTICAL	S 178
C	BODY LOCATIONS AND DETERMINE NEW CORRECTION	S 179
C		S 180
	IF (NHC.EQ.1) GC TO 34	S 181
	IF (R1.EQ.0.0) GC TO 19	S 182
	IF (R1.GT.0..AND.NP.EQ.0) GO TO 30	S 183
	IF (NP.EQ.1) GC TO 35	S 184
19	GO TO (20,21,22,23), L	S 185
20	B3=((ZST+RKBN)-ZIC(4,NT1))**2	S 186
	RW4C=SQRT((RKBN**2)-B3)	S 187
	GO TO 24	S 188
21	B3=((ZST+ABA)-ZIC(4,NT1))**2	S 189
	RW4C=(ABB/ABA)*SQRT((ABA**2)-B3)	S 190
	GO TO 24	S 191
22	RW4C=SQRT(2.*F1*(ZIC(4,NT1)-ZST))	S 192
	GO TO 24	S 193
23	B3=(ZIC(4,NT1)*(HPA-ZST))**2	S 194
	RW4C=(HPB/HPA)*SQRT(B3-(HPA**2))	S 195
24	E4(IT)=((RIC(4,NT1)/RW4C)-1.)*100.	S 196
	IF (ABS(E4(IT)).GT.EM) GC TO 30	S 197
	ISUM=ISUM+1	S 198
	I=ISUM	S 199

APPENDIX B - Continued

	GO TO (27,25,25,28), L	S 200
25	THB(I)=ATAN(P1/RIC(4,NT1))	S 201
	GO TO 29	S 202
26	THB(I)=ATAN(((ABB/ABA)**2)*(ABA-ZIC(4,NT1)+ZST)/RIC(4,NT1))	S 203
	GO TO 29	S 204
27	THB(I)=ATAN((RKBN-(ZIC(4,NT1)-ZST))/RIC(4,NT1))	S 205
	GO TO 29	S 206
28	THB(I)=ATAN(((HPB/HPA)**2)*(HPA+ZIC(4,NT1)-ZST)/RIC(4,NT1))	S 207
29	IF (THC.EQ.0..AND.IOPT.EQ.1) GO TO 31	S 208
	IF (IOPT.EQ.0) GO TO 42	S 209
	RB(ISUM)=RIC(4,NT1)	S 210
	ZB(ISUM)=ZIC(4,NT1)	S 211
	IF (THB(ISUM).GT.THG) GO TO 42	S 212
	CALL FTLUP (THC,R1,1,ISUM,THB,RB)	S 213
	CALL FTLUP (THC,Z2,1,ISUM,THB,ZB)	S 214
	DETC=DETH	S 215
C		S 216
C	THE BODY-CCNE JUNCTURE IS LOCATED.R1 AND Z2 ARE THE RADIAL AND AXI	S 217
C	AL LOCATIONS RESPECTIVELY OF THE JUNCTURE POINT.	S 218
C		S 219
	WRITE (6,55)	S 220
	DETH=DETH*(R1-RB(ISUM-1))/(RB(ISUM)-RB(ISUM-1))	S 221
	DR(1)=.5*CR(IT)	S 222
	IT=1	S 223
	GO TO 3	S 224
30	RW4C=R1	S 225
	E4(IT)=((RIC(4,NT1)/RW4C)-1.0)*100.	S 226
	IF (ABS(E4(IT)).GT.EM) GO TO 36	S 227
	NP=1	S 228
	DETH=DETC	S 229
C		S 230
C	THE BODY-CONE JUNCTURE AND RESPECTIVE SHOCK POINT ARE LOCATED.	S 231
C	THE PROPERTIES ALONG RAY INTERSECTING JUNCTURE POINT ARE COMPUTED.	S 232
C		S 233
	GO TO 42	S 234
31	IF (NH.EQ.1) GO TO 32	S 235
C		S 236
C	BODY-CYLINDER JUNCTURE IS COMPUTED.NOTE---IN THE FOLLOWING STATE	S 237
C	MENTS THE FIRST,SEVENTH,AND EIGHT SHOULD BE CHANGED IF BODY OTHER	S 238
C	THAN A SPHERE IS CONSIDERED.	S 239
C		S 240
	IF ((RKBN+ZST-ZIC(4,NT1)).GT.0.) GO TO 42	S 241
	DETHB=DETH	S 242
	NH=1	S 243
	DETH=.5*DETH	S 244
	DR(1)=.5*CR(IT)	S 245
	IT=1	S 246
	GO TO 3	S 247
32	IF ((RKBN+ZST-ZIC(4,NT1)).GT..0001) GO TO 42	S 248
	IF (ABS(RKBN+ZST-ZIC(4,NT1)).LE..0001) GO TO 34	S 249
	IF (NHH.EQ.1) GO TO 33	S 250
	DR(1)=.5*CR(IT)	S 251
	IT=1	S 252
	DETH=.2*DETH	S 253
	NHH=1	S 254
	GO TO 3	S 255
33	DR(1)=.2*CR(IT)	S 256
	DETH=.1*DETH	S 257
	IT=1	S 258
	GO TO 3	S 259
34	E4(IT)=((RIC(4,NT1)/RW4C)-1.)*100.	S 260
	IF (ABS(E4(IT)).GT.EM) GO TO 36	S 261
	NHC=1	S 262
	ICOUNT=ICOUNT+1	S 263
	RW4C=RKBN	S 264
	GO TO 42	S 265

APPENDIX B - Continued

C		S 266
C	IF BODY OTHER THAN A SPHERE IS CONSIDERED, APPROPRIATE CROSS SECTIONAL BODY RADIUS AT JUNCTURE SHOULD BE USED.	S 267
C		S 268
C		S 269
35	CONTINUE	S 270
C		S 271
C	THE FOLLOWING STATEMENTS COMPUTE CONE GEOMETRY.	S 272
C		S 273
	ZC=ZIC(4,NT1)-Z2	S 274
	RT=ZC*TAN(THC)	S 275
	RW4C=R1+RT	S 276
	E4(IT)=(RIC(4,NT1)/RW4C)-1.0)*100.	S 277
	IF (IZ.EQ.1) EM=.001	S 278
	IF (ABS(E4(IT)).LE.EM) GO TO 42	S 279
36	CONTINUE	S 280
C		S 281
C	THE FOLLOWING STATEMENTS COMPUTE CORRECTION TO RADIUS OF CURVATURE	S 282
C		S 283
	IF (IT.GE.2) GO TO 40	S 284
	IF (IZ.EQ.1) GO TO 37	S 285
	IF (E4(IT).GT.0.0) GO TO 39	S 286
	GO TO 38	S 287
37	IF (E4(IT).GT.0..AND.DR(IT).GT.0.) GO TO 39	S 288
	IF (E4(IT).LT.0..AND.DR(IT).LT.0.) GO TO 39	S 289
38	IT=IT+1	S 290
	DR(IT)=DR(IT-1)*2.	S 291
	GO TO 3	S 292
39	IT=IT+1	S 293
	DR(IT)=DR(IT-1)-0.50*DR(IT-1)	S 294
	GO TO 3	S 295
40	IT=IT+1	S 296
	ID=ID+1	S 297
	IF (IZ.EQ.1.AND.ID.GE.18.AND.E4(IT-1).LT..02) GO TO 42	S 298
	IF (ID.GE.8.AND.RKSX(ND).GT.3000.) GO TO 41	S 299
	IF (RKSX(ND).GT.10000.) GO TO 41	S 300
	IF (E4(IT-1).EQ.E4(IT-2).AND.NP.EQ.1) GO TO 49	S 301
	IF (IT.EQ.9) E4(1)=E4(7)	S 302
	IF (IT.EQ.9) E4(2)=E4(8)	S 303
	IF (IT.EQ.9) DR(2)=DR(8)	S 304
	IF (IT.EQ.9) DR(1)=DR(7)	S 305
	IF (IT.EQ.9) IT=3	S 306
	DR(IT)=DR(IT-1)-E4(IT-1)*(DR(IT-1)-DR(IT-2))/(E4(IT-1)-E4(IT-2))	S 307
	GO TO 3	S 308
41	IF (RKSX(ND).GT.10.) DR(1)=.1*RKSX(ND)	S 309
	IF (RKSX(ND).LT.10.) DR(1)=-1.	S 310
	DETH=-DTHC	S 311
	RKSX(ND)=-RKSX(ND)	S 312
	IZ=1	S 313
	IT=1	S 314
	GO TO 3	S 315
42	CONTINUE	S 316
C		S 317
C	THE FOLLOWING STATEMENTS CALL ROUTINE TO WRITE CONVERGED RESULTS	S 318
C	AND INITIALIZE DATA TO GO TO NEW POSITION ON SHOCK.	S 319
C		S 320
	CALL OUTPUTS	S 321
	IF (RS(ND).GT.READ) GO TO 54	S 322
	IF (THC.EQ.0..AND.IOPT.EQ.1) GO TO 44	S 323
	IF (RHS.GT.0.) GO TO 44	S 324
	IF (IZ.EQ.1) GO TO 46	S 325
	IF (THETAS(ND).LT.THSC) GO TO 43	S 326
	GO TO 44	S 327
43	CALL FTLUP (THSC,RHS,1,NC,THETAS,RHCS)	S 328
	CALL FTLUP (THSC,USN,1,NC,THETAS,US)	S 329
	CALL FTLUP (THSC,PSN,1,NC,THETAS,PS)	S 330
44	IF (RKSX(ND).GT.10.) GO TO 46	S 331

APPENDIX B - Continued

	IF (ICOUNT.EQ.4.AND.DETH.GT..5*DETHB) DETH=.5*DETHB	S 332
	IF (ICOUNT.GE.1.AND.ICOUNT.LT.4) GO TO 45	S 333
	DR(1)=.1	S 334
	GO TO 46	S 335
45	DR(1)=DR(IT)	S 336
46	IF (RKXS(ND).GT.10.) DR(1)=0.1*RKXS(ND)	S 337
	DTHC=DETH	S 338
	IF (RKXS(ND).LT.0..AND.RKXS(ND).GT.-10.) DR(1)=-.15	S 339
	IF (RKXS(ND).LT.-10.) DR(1)=.1*RKXS(ND)	S 340
	IF (RKXS(ND).LT.1000.) GO TO 47	S 341
	IF (IZ.EQ.1) GO TO 47	S 342
	IZ=1	S 343
	DETH=-DETH	S 344
	RKXS(ND)=-RKXS(ND)	S 345
	DR(1)=-DR(IT)	S 346
47	IF (IZ.EQ.1.AND.ABS(THETAS(ND)-THSC).LT..001) GO TO 49	S 347
	IF (IZ.EQ.1.AND.(THETAS(ND)-THSC).GT..001) GO TO 49	S 348
	IF (IZ.EQ.1.AND.RKXS(ND).GT.0.) DR(1)=-.1*RKXS(ND)	S 349
	IF (IZ.EQ.1.AND.DETH.LT..001) DETH=-.1*DETH	S 350
	IF (IZ.EQ.1.AND.RKXS(ND).LT.-5000.) GO TO 48	S 351
	IT=1	S 352
	NC=ND	S 353
	GO TO 2	S 354
48	THS1=THETAS(ND)	S 355
49	CONTINUE	S 356
	NC=ND	S 357
	NB=NC	S 358
	ZN=ZS(NC)	S 359
	RN=RS(NC)	S 360
	YC=YI(4,NT1)	S 361
	RHOS(NB)=RHS	S 362
	US(NB)=USN	S 363
	PS(NB)=PSN	S 364
	IF (THS1.GT.0.) THS=THS1	S 365
	IF (THS1.EQ.0.) THS=THSC	S 366
	XEFF=RN/SIN(THS)	S 367
	SIG=THS-THC	S 368
	YDC=XEFF*TAN(SIG)	S 369
	YTM=YC-YDC	S 370
	ISUM=0	S 371
50	I=NC+1	S 372
	NZ=2+ISUM	S 373
	IF (THS1.GT.0..AND.NZ.GT.5) THS=.5*(THSC+THS1)	S 374
	RS1=NZ*(.15)	S 375
	RS(I)=RN+RS1	S 376
	ZS(I)=ZN+(RS1/TAN(THS))	S 377
	SFS(I)=0.5*RS(I)**2	S 378
	SIGMA=THETA1N-THS	S 379
	DSY=SFS(I)/NT1	S 380
	XS(I)=XEFF+(RS1/SIN(THS))	S 381
	DO 51 J=1,NT1	S 382
	SY(4,J)=SFS(I)-J*DSY	S 383
	YI(4,J)=(1.0/(RHOS(NB)*US(NB)*RS(I)))*(SFS(I)-SY(4,J))	S 384
51	CONTINUE	S 385
	YI(4,NT1)=YI(4,NT1)+YTM	S 386
	YL=YI(4,NT1)/NT1	S 387
	DO 52 J=1,NT1	S 388
	YI(4,J)=J*YL	S 389
52	CONTINUE	S 390
	DO 53 J=1,NT1	S 391
	RI(4,J)=RS(I)-COS(THS)*YI(4,J)	S 392
	RP=RS(I)-RI(4,J)	S 393
	ZI(4,J)=ZS(I)+(RP/TAN(SIGMA))	S 394
	PI(4,J)=PS(NB)+(1.0/(RHOS(NB)*(RS(I)**2)*XS(I)**2))*((SFS(I)**2)-S	S 395
	1Y(4,J)**2)	S 396
53	CONTINUE	S 397

APPENDIX B - Continued

```

ROC(4)=RS(I)
ZCC(4)=ZS(I)
RIC(4,NT1)=RI(4,NT1)
YIC(4,NT1)=YI(4,NT1)
ZIC(4,NT1)=ZI(4,NT1)
CALL OUTPUTS
IF (RS(I).GT.REND) GO TO 54
ISUM=ISUM+1
NC=I
GO TO 50
54 RETURN
C
55 FORMAT (//2X,31H BODY CONE JUNCTURE IS LOCATED )
END

```

S 398
S 399
S 400
S 401
S 402
S 403
S 404
S 405
S 406
S 407
S 408
S 409
S 410
S 411-

```

SUBROUTINE OUTPUTS
C
C THIS SUBROUTINE WRITES THE SOLUTIONS FOR SUPERSONIC FLOW FIELD
C
COMMON /BLK2/ IT,DELX,IBEG,EM,NC,NT1,NX,REND,ND,PST,DR(8),F(200),I
1P
COMMON /BLK4/ XS(300),RKSX(300),ZS(300),RS(300),SFS(300),THETAS(30
10),US(300),PS(300),RHOS(300),MS(300),VS(300)
COMMON /BLK5/ RI(7,15),ZI(7,15),YI(7,15),RIC(7,15),ZIC(7,15),YIC(7
1,15),RW4C,ZST,E4(8),THB(50)
COMMON /BLK6/ SFC(7),RO(7),ZO(7),PO(7),UO(7),THETAO(7),RHOSC(7),MS
10(7),RKO(7),DELSY(7),RKOC(7),ROC(7),ZOC(7),VO(7)
COMMON /BLK7/ SY(7,15),PI(7,15),RHI(7,15),UI(7,15),MSI(7,15),VI(7,
115)
IF (IC.EQ.2) GO TO 1
IB=NX-1
1 IB=IB+1
IC=2
WRITE (6,2) ZIC(4,NT1),RIC(4,NT1),YIC(4,NT1),ZCC(4),ROC(4),ND
WRITE (6,3) PS(ND),RHOS(ND),US(ND),PI(4,NT1),RHI(4,NT1),UI(4,NT1),
1MSI(4,NT1),THB(18)
RETURN
C
2 FORMAT (//2X,3HZH=,E11.4,2X,3HRW=,E11.4,2X,3HYW=,E11.4,2X,3HZS=,E1
11.4,2X,3HRS=,E11.4,15)
3 FORMAT (2X,3HPS=,E11.4,2X,5HRHOS=,E11.4,2X,3HUS=,E11.4,2X,3HPW=,E1
11.4,2X,5HRHCW=,E11.4,2X,3HUM=,E11.4,2X,3HMM=,E11.4,2X,4HTHB=,E11.
24)
END

```

T 1
T 2
T 3
T 4
T 5
T 6
T 7
T 8
T 9
T 10
T 11
T 12
T 13
T 14
T 15
T 16
T 17
T 18
T 19
T 20
T 21
T 22
T 23
T 24
T 25
T 26
T 27
T 28
T 29-

The sample output is for a paraboloid at $M_\infty = 10$ and $\gamma = 1.4$.

STAG PT SHK RAD CUR = 1.4216E+00 STAG PT STAND OFF DIST = 1.4743E-01
BODY STAG PT PRESS= 9.2298E-01

ARC LENGTH	SHOCK AXIAL LOC	SHOCK RADIAL LOC	BODY AXIAL LOC	BODY RADIAL LOC	BODY NGRMAL LOC	SHOCK RADIUS OF CURV
1.5077E-01	7.9916E-03	1.5049E-01	1.5616E-01	1.3483E-01	1.4899E-01	1.4513E+00
3.0155E-01	3.1489E-02	2.5935E-01	1.8323E-01	2.6756E-01	1.5504E-01	1.5395E+00
4.5232E-01	6.9379E-02	4.4522E-01	2.2606E-01	3.5670E-01	1.6402E-01	1.6865E+00
6.0309E-01	1.2013E-01	5.6715E-01	2.8220E-01	5.2108E-01	1.7555E-01	1.8922E+00
7.5387E-01	1.8201E-01	7.2460E-01	3.5245E-01	6.4022E-01	1.9019E-01	2.1567E+00
9.0464E-01	2.5335E-01	8.5739E-01	4.3174E-01	7.5407E-01	2.0616E-01	2.4799E+00

APPENDIX B - Continued

XSP= 4.5232E-01

7.6636E-01	5.7050E+00	2.9070E-01	1.5870E-01	7.6371E-01	9.2576E-02
7.7287E-01	5.7176E+00	2.8550E-01	1.4926E-01	7.4056E-01	8.5964E-02
7.7870E-01	5.7262E+00	2.8032E-01	1.3960E-01	7.1771E-01	7.9351E-02
7.8386E-01	5.7308E+00	2.7516E-01	1.2968E-01	6.9514E-01	7.2739E-02
7.8834E-01	5.7315E+00	2.6999E-01	1.1950E-01	6.7284E-01	6.6126E-02
7.9215E-01	5.7284E+00	2.6479E-01	1.0902E-01	6.5081E-01	5.9513E-02
7.9528E-01	5.7215E+00	2.5952E-01	9.8231E-02	6.2903E-01	5.2901E-02
7.9774E-01	5.7108E+00	2.5415E-01	8.7056E-02	6.0751E-01	4.6288E-02
7.9953E-01	5.6966E+00	2.4863E-01	7.5595E-02	5.8625E-01	3.9676E-02
8.0063E-01	5.6786E+00	2.4292E-01	6.3705E-02	5.6525E-01	3.3063E-02
8.0107E-01	5.6571E+00	2.3693E-01	5.1411E-02	5.4452E-01	2.6450E-02
8.0082E-01	5.6321E+00	2.3060E-01	3.8716E-02	5.2407E-01	1.9838E-02
7.9991E-01	5.6035E+00	2.2381E-01	2.5664E-02	5.0392E-01	1.3225E-02
7.9831E-01	5.5715E+00	2.1646E-01	1.2425E-02	4.8410E-01	6.6126E-03
7.9605E-01	5.5361E+00	2.0847E-01	0.	4.6463E-01	4.4409E-03

MACH NO WL	SHOCK PRESSURE,	TAN SHK VELOCITY	ACR SHK VELOCITY	SHOCK DENSITY,	SHOCK MACH NUMB	BODY ANGLE
1.7362E-01	8.2250E-01	1.0512E-01	1.7412E-01	5.7112E+00	4.5304E-01	1.4368E+00
3.2186E-01	7.5706E-01	2.0502E-01	1.7164E-01	5.7023E+00	6.0457E-01	1.3094E+00
4.6463E-01	7.5918E-01	2.5982E-01	1.6793E-01	5.6883E+00	7.8772E-01	1.1931E+00
5.9658E-01	7.1463E-01	3.7547E-01	1.6346E-01	5.6700E+00	9.7454E-01	1.0904E+00
7.1576E-01	6.6609E-01	4.4367E-01	1.5866E-01	5.6484E+00	1.1579E+00	1.0013E+00
8.2180E-01	6.2280E-01	5.0121E-01	1.5385E-01	5.6244E+00	1.3316E+00	9.2470E-01

XSP= 1.5077E-01

FIELD PRESSURE	FIELD DENSITY	FIELD VELOCITY(TANG)	FIELD VELOCITY(NGRM)	FIELD MACH NO	FIELD STRM FUNC
8.3366E-01	5.7617E+00	1.0156E-01	1.6366E-01	4.2832E-01	1.0612E-02
8.4366E-01	5.8061E+00	9.8333E-02	1.5342E-01	4.0409E-01	9.8537E-03
8.5289E-01	5.8505E+00	9.5646E-02	1.4275E-01	3.8043E-01	9.0957E-03
8.6135E-01	5.8890E+00	9.3451E-02	1.3197E-01	3.5735E-01	8.3377E-03
8.6904E-01	5.9236E+00	9.1696E-02	1.2095E-01	3.3490E-01	7.5757E-03
8.7597E-01	5.9543E+00	9.0316E-02	1.0972E-01	3.1313E-01	6.8218E-03
8.8212E-01	5.9812E+00	8.9237E-02	9.8265E-02	2.9212E-01	6.0638E-03
8.8752E-01	6.0043E+00	8.8376E-02	8.6543E-02	2.7157E-01	5.3058E-03
8.9214E-01	6.0236E+00	8.7638E-02	7.4660E-02	2.5283E-01	4.5478E-03
8.9600E-01	6.0392E+00	8.6917E-02	6.2490E-02	2.3489E-01	3.7899E-03
8.9908E-01	6.0511E+00	8.6057E-02	5.0073E-02	2.1838E-01	3.0319E-03
9.0141E-01	6.0592E+00	8.5049E-02	3.7426E-02	2.0361E-01	2.2739E-03
9.0296E-01	6.0636E+00	8.3638E-02	2.4616E-02	1.9095E-01	1.5159E-03
9.0375E-01	6.0644E+00	8.1737E-02	1.1820E-02	1.8081E-01	7.5757E-04
9.0376E-01	6.0614E+00	7.9323E-02	0.	1.7362E-01	5.5511E-04

FIELD NORMAL LOC	FIELD AXIAL LOC	FIELD RADIAL LOC
8.5231E-03	1.6467E-02	1.4959E-01
1.7318E-02	2.5213E-02	1.4867E-01
2.6368E-02	3.4214E-02	1.4772E-01
3.5648E-02	4.3442E-02	1.4674E-01
4.5131E-02	5.2872E-02	1.4575E-01
5.4789E-02	6.2478E-02	1.4473E-01
6.4601E-02	7.2235E-02	1.4370E-01
7.4550E-02	8.2123E-02	1.4265E-01
8.4627E-02	9.2149E-02	1.4159E-01
9.4834E-02	1.0230E-01	1.4052E-01
1.0519E-01	1.1260E-01	1.3943E-01
1.1572E-01	1.2307E-01	1.3833E-01
1.2647E-01	1.3376E-01	1.3720E-01
1.3753E-01	1.4476E-01	1.3603E-01
1.4899E-01	1.5616E-01	1.3483E-01

XSP= 3.0155E-01

8.0630E-01	5.7389E+00	2.0072E-01	1.6155E-01	5.8152E-01	4.1886E-02
8.1480E-01	5.7713E+00	1.9647E-01	1.5207E-01	5.5883E-01	3.6894E-02
8.2257E-01	5.7957E+00	1.9242E-01	1.4198E-01	5.3665E-01	3.5902E-02
8.2962E-01	5.8242E+00	1.8857E-01	1.3166E-01	5.1500E-01	3.2910E-02
8.3594E-01	5.8448E+00	1.8487E-01	1.2105E-01	4.9388E-01	2.9918E-02
8.4153E-01	5.8616E+00	1.8131E-01	1.1025E-01	4.7332E-01	2.6926E-02
8.4639E-01	5.8745E+00	1.7785E-01	9.9122E-02	4.5335E-01	2.3935E-02
8.5052E-01	5.8838E+00	1.7444E-01	8.7689E-02	4.3400E-01	2.0944E-02
8.5393E-01	5.8893E+00	1.7103E-01	7.5927E-02	4.1533E-01	1.7951E-02
8.5660E-01	5.8911E+00	1.6755E-01	6.3822E-02	3.9735E-01	1.4959E-02
8.5855E-01	5.8852E+00	1.6393E-01	5.1366E-02	3.8026E-01	1.1967E-02
8.5977E-01	5.8837E+00	1.6007E-01	3.8570E-02	3.6403E-01	8.9755E-03
8.6026E-01	5.8746E+00	1.5586E-01	2.5487E-02	3.4860E-01	5.9836E-03
8.6002E-01	5.8619E+00	1.5119E-01	1.2297E-02	3.3470E-01	2.9918E-03
8.5905E-01	5.8457E+00	1.4599E-01	0.	3.2186E-01	2.2204E-03

APPENDIX B - Continued

FIELD NORMAL LOC	FIELD AXIAL LOC	FIELD RADIAL LOC
8.6366E-03	3.5938E-02	2.9754E-01
1.7460E-02	4.8574E-02	2.9577E-01
2.6481E-02	5.7403E-02	2.9392E-01
3.5705E-02	6.6431E-02	2.9203E-01
4.5140E-02	7.5666E-02	2.9010E-01
5.4797E-02	8.5118E-02	2.8812E-01
6.4685E-02	9.4796E-02	2.8609E-01
7.4820E-02	1.0472E-01	2.8401E-01
8.5219E-02	1.1489E-01	2.8188E-01
9.5904E-02	1.2535E-01	2.7969E-01
1.0690E-01	1.3612E-01	2.7743E-01
1.1826E-01	1.4723E-01	2.7511E-01
1.3002E-01	1.5874E-01	2.7270E-01
1.4225E-01	1.7071E-01	2.7019E-01
1.5504E-01	1.8323E-01	2.6757E-01

FIELD NORMAL LOC	FIELD AXIAL LOC	FIELD RADIAL LOC
8.9160E-03	7.7846E-02	4.4259E-01
1.8024E-02	8.6596E-02	4.3989E-01
2.7339E-02	9.5494E-02	4.3714E-01
3.6877E-02	1.0461E-01	4.3432E-01
4.6655E-02	1.1395E-01	4.3142E-01
5.6694E-02	1.2354E-01	4.2845E-01
6.7013E-02	1.3339E-01	4.2540E-01
7.7640E-02	1.4354E-01	4.2226E-01
8.8603E-02	1.5402E-01	4.1901E-01
9.9937E-02	1.6484E-01	4.1566E-01
1.1166E-01	1.7606E-01	4.1219E-01
1.2339E-01	1.8773E-01	4.0857E-01
1.3663E-01	1.9989E-01	4.0481E-01
1.4947E-01	2.1264E-01	4.0086E-01
1.6402E-01	2.2606E-01	3.9670E-01

XSP= 6.0309E-01

7.1966E-01	5.6644E+00	3.8975E-01	1.5471E-01	9.5035E-01	1.6094E-01
7.2408E-01	5.6546E+00	3.8385E-01	1.4574E-01	9.2572E-01	1.4944E-01
7.2789E-01	5.6407E+00	3.5786E-01	1.3653E-01	9.0112E-01	1.3795E-01
7.3107E-01	5.6228E+00	3.5173E-01	1.2705E-01	8.7654E-01	1.2645E-01
7.3365E-01	5.6010E+00	3.4545E-01	1.1725E-01	8.5193E-01	1.1496E-01
7.3561E-01	5.5753E+00	3.3900E-01	1.0722E-01	8.2727E-01	1.0346E-01
7.3695E-01	5.5458E+00	3.3233E-01	9.6804E-02	8.0252E-01	9.1966E-02
7.3768E-01	5.5127E+00	3.2541E-01	8.6021E-02	7.7765E-01	8.0470E-02
7.3719E-01	5.4758E+00	3.1819E-01	7.4840E-02	7.5261E-01	6.8975E-02
7.3729E-01	5.4354E+00	3.1061E-01	6.3232E-02	7.2738E-01	5.7479E-02
7.3617E-01	5.3914E+00	3.0259E-01	5.1173E-02	7.0191E-01	4.5983E-02
7.3444E-01	5.3440E+00	2.9406E-01	3.8655E-02	6.7615E-01	3.4467E-02
7.3209E-01	5.2931E+00	2.8489E-01	2.5710E-02	6.5005E-01	2.2992E-02
7.2913E-01	5.2389E+00	2.7456E-01	1.2494E-02	6.2355E-01	1.1496E-02
7.2555E-01	5.1813E+00	2.6415E-01	0.	5.9658E-01	8.8818E-16

FIELD NORMAL LOC	FIELD AXIAL LOC	FIELD RADIAL LOC
9.2586E-03	1.2874E-01	5.8366E-01
1.6815E-02	1.3156E-01	5.8009E-01
2.8589E-02	1.4660E-01	5.7642E-01
3.8543E-02	1.5589E-01	5.7266E-01
4.8878E-02	1.6543E-01	5.6880E-01
5.9483E-02	1.7526E-01	5.6482E-01
7.0426E-02	1.8540E-01	5.6071E-01
8.1745E-02	1.9589E-01	5.5646E-01
9.3473E-02	2.0676E-01	5.5205E-01
1.0566E-01	2.1806E-01	5.4748E-01
1.1837E-01	2.2983E-01	5.4271E-01
1.3166E-01	2.4215E-01	5.3772E-01
1.4561E-01	2.5508E-01	5.3248E-01
1.6033E-01	2.6872E-01	5.2695E-01
1.7595E-01	2.8320E-01	5.2109E-01

XSP= 7.5387E-01

6.7117E-01	5.6207E+00	4.3761E-01	1.5039E-01	1.1317E+00	2.4506E-01
6.7370E-01	5.5887E+00	4.3132E-01	1.4188E-01	1.1053E+00	2.2755E-01
6.7567E-01	5.5525E+00	4.2481E-01	1.3313E-01	1.0786E+00	2.1005E-01
6.7709E-01	5.5123E+00	4.1805E-01	1.2411E-01	1.0516E+00	1.9254E-01
6.7795E-01	5.4681E+00	4.1102E-01	1.1478E-01	1.0243E+00	1.7504E-01
6.7826E-01	5.4199E+00	4.0367E-01	1.0513E-01	9.9658E-01	1.5754E-01
6.7801E-01	5.3679E+00	3.9557E-01	9.5118E-02	9.6841E-01	1.4003E-01
6.7720E-01	5.3120E+00	3.8785E-01	8.4715E-02	9.3971E-01	1.2253E-01
6.7584E-01	5.2525E+00	3.7927E-01	7.3886E-02	9.1041E-01	1.0502E-01
6.7393E-01	5.1894E+00	3.7015E-01	6.2594E-02	8.8041E-01	8.7520E-02
6.7146E-01	5.1226E+00	3.6039E-01	5.0808E-02	8.4962E-01	7.0016E-02
6.6843E-01	5.0524E+00	3.4989E-01	3.8507E-02	8.1791E-01	5.2512E-02
6.6485E-01	4.9788E+00	3.3850E-01	2.5707E-02	7.8514E-01	3.5008E-02
6.6072E-01	4.9018E+00	3.2606E-01	1.2546E-02	7.5116E-01	1.7504E-02
6.5602E-01	4.8216E+00	3.1239E-01	0.	7.1576E-01	1.7764E-15

APPENDIX B – Concluded

FIELD NORMAL LUC	FIELD AXIAL LUC	FIELD RADIAL LUC			
9.7579E-03	1.9075E-01	7.2027E-01			
1.9768E-02	1.9972E-01	7.1583E-01			
3.0055E-02	2.0894E-01	7.1126E-01			
4.0644E-02	2.1843E-01	7.0657E-01			
5.1566E-02	2.2822E-01	7.0172E-01			
6.2854E-02	2.3834E-01	6.9671E-01			
7.4546E-02	2.4881E-01	6.9152E-01			
8.6687E-02	2.5970E-01	6.8614E-01			
9.9329E-02	2.7102E-01	6.8053E-01			
1.1253E-01	2.8286E-01	6.7467E-01			
1.2637E-01	2.9526E-01	6.6853E-01			
1.4093E-01	3.0831E-01	6.6207E-01			
1.5632E-01	3.2210E-01	6.5524E-01			
1.7268E-01	3.3676E-01	6.4794E-01			
1.9019E-01	3.5245E-01	6.4022E-01			
XSP= 9.0464E-01					
6.2427E-01	5.5767E+00	4.9505E-01	1.4602E-01	1.3038E+00	3.4306E-01
6.2524E-01	5.5245E+00	4.8861E-01	1.3797E-01	1.2755E+00	3.1856E-01
6.2572E-01	5.461E+00	4.8189E-01	1.2965E-01	1.2467E+00	2.9405E-01
6.2569E-01	5.4074E+00	4.7475E-01	1.2106E-01	1.2173E+00	2.6955E-01
6.2516E-01	5.3426E+00	4.6725E-01	1.1216E-01	1.1872E+00	2.4504E-01
6.2413E-01	5.2737E+00	4.5932E-01	1.0292E-01	1.1564E+00	2.2054E-01
6.2261E-01	5.2009E+00	4.5089E-01	9.3314E-02	1.1247E+00	1.9603E-01
6.2058E-01	5.1240E+00	4.4191E-01	8.3295E-02	1.0921E+00	1.7153E-01
6.1805E-01	5.0434E+00	4.3227E-01	7.2827E-02	1.0583E+00	1.4703E-01
6.1503E-01	4.9589E+00	4.2190E-01	6.1866E-02	1.0233E+00	1.2252E-01
6.1150E-01	4.8707E+00	4.1066E-01	5.0371E-02	9.8687E-01	9.8017E-02
6.0747E-01	4.7790E+00	3.9841E-01	3.8307E-02	9.4879E-01	7.3513E-02
6.0295E-01	4.6836E+00	3.8496E-01	2.5675E-02	9.0881E-01	4.9008E-02
5.9792E-01	4.5849E+00	3.7008E-01	1.2587E-02	8.6661E-01	2.4504E-02
5.9239E-01	4.4827E+00	3.5348E-01	0.	8.2180E-01	1.7764E-02
FIELD NORMAL LUC	FIELD AXIAL LUC	FIELD RADIAL LUC			
1.0274E-02	2.6224E-01	8.5225E-01			
2.0839E-02	2.7138E-01	8.4655E-01			
3.1721E-02	2.8080E-01	8.4150E-01			
4.2954E-02	2.9052E-01	8.3587E-01			
5.4573E-02	3.0057E-01	8.3004E-01			
6.6621E-02	3.1100E-01	8.2400E-01			
7.9144E-02	3.2183E-01	8.1773E-01			
9.2196E-02	3.3313E-01	8.1118E-01			
1.0585E-01	3.4494E-01	8.0434E-01			
1.2017E-01	3.5734E-01	7.9710E-01			
1.3527E-01	3.7040E-01	7.8960E-01			
1.5125E-01	3.8423E-01	7.8159E-01			
1.6826E-01	3.9894E-01	7.7306E-01			
1.8648E-01	4.1471E-01	7.6393E-01			
2.0616E-01	4.3174E-01	7.54907E-01			
ZW= 5.0366E-01	RW= 8.4407E-01	YW= 2.2055E-01	ZS= 3.1834E-01	RS= 9.6364E-01	43
PS= 5.8720E-01	RHUS= 5.0032E+00	US= 5.4215E-01	PH= 5.4298E-01	RHUN= 4.2124E+00	UW= 3.843CE-01
THB= 8.6975E-01					MW= 9.0463E-01
ZW= 5.8532E-01	RW= 9.5583E-01	YW= 2.3658E-01	ZS= 3.9475E-01	RS= 1.0732E+00	50
PS= 5.5097E-01	RHUS= 5.5790E+00	US= 5.8087E-01	PH= 4.9367E-01	RHUN= 3.9354E+00	UW= 4.1460E-01
THB= 8.1853E-01					MW= 9.8934E-01
ZW= 6.7697E-01	RW= 1.0251E+00	YW= 2.5412E-01	ZS= 4.7687E-01	RS= 1.1858E+00	57
PS= 5.1548E-01	RHUS= 5.5522E+00	US= 6.1644E-01	PH= 4.5097E-01	RHUN= 3.6891E+00	UW= 4.4080E-01
THB= 7.7105E-01					MW= 1.0655E+00
ZW= 7.8124E-01	RW= 1.1259E+00	YW= 2.7261E-01	ZS= 5.7311E-01	RS= 1.3035E+00	64
PS= 4.8104E-01	RHUS= 5.5228E+00	US= 6.4909E-01	PH= 4.1071E-01	RHUN= 3.4508E+00	UW= 4.6565E-01
THB= 7.2625E-01					MW= 1.1408E+00
ZW= 8.9862E-01	RW= 1.2257E+00	YW= 2.9506E-01	ZS= 6.8200E-01	RS= 1.4261E+00	71
PS= 4.4799E-01	RHUS= 5.4507E+00	US= 6.7896E-01	PH= 3.7355E-01	RHUN= 3.2248E+00	UW= 4.8901E-01
THB= 6.8433E-01					MW= 1.2143E+00
ZW= 1.0298E+00	RW= 1.3285E+00	YW= 3.1853E-01	ZS= 8.0432E-01	RS= 1.5534E+00	78
PS= 4.1652E-01	RHUS= 5.4558E+00	US= 7.0622E-01	PH= 3.3536E-01	RHUN= 3.0111E+00	UW= 5.1095E-01
THB= 6.4526E-01					MW= 1.2863E+00

REFERENCES

1. Hayes, Wallace D.; and Probstein, Ronald F.: Hypersonic Flow Theory. Vol. 1 - Inviscid Flows. Second ed., Academic Press, Inc., 1966.
2. Grose, William Lyman: An Approximate Solution to the Nonequilibrium Flow in the Inviscid Shock Layer About a Vehicle in Hypersonic Flight in an Arbitrary Atmosphere. Ph. D. Thesis, Virginia Polytech. Inst., June 1969.
3. Maslen, S. H.: Inviscid Hypersonic Flow Past Smooth Symmetric Bodies. AIAA J., vol. 2, no. 6, June 1964, pp. 1055-1061.
4. Jackson, Sherman Keith, Jr.: The Viscous-Inviscid Hypersonic Flow of a Perfect Gas Over Smooth Symmetric Bodies. Ph. D. Thesis, Univ. of Colorado, 1966.
5. Maslen, Stephen H.: Asymmetric Hypersonic Flow. NASA CR-2123, 1972.
6. Van Dyke, Milton D.; and Gordon, Helen D.: Supersonic Flow Past a Family of Blunt Axisymmetric Bodies. NASA TR R-1, 1959.
7. Holt, Maurice; and Hoffman, Gilbert H.: Calculation of Hypersonic Flow Past Spheres and Ellipsoids. [Preprint] 61-209-1903, American Rocket Soc., June 1961.
8. Mangler, K. W.: The Calculation of the Flow Field Between a Blunt Body and the Bow Wave: Hypersonic Flow. A. R. Collar and J. Tinkler, eds., Academic Press, Inc., 1960, pp. 219-237.
9. Inouye, Mamoru; and Lomax, Harvard: Comparison of Experimental and Numerical Results for the Flow of a Perfect Gas About Blunt-Nosed Bodies. NASA TN D-1426 1962.
10. Inouye, Mamoru; Rakich, John V.; and Lomax, Harvard: A Description of Numerical Methods and Computer Programs for Two-Dimensional and Axisymmetric Supersonic Flow Over Blunt-Nosed and Flared Bodies. NASA TN D-2970, 1965.
11. Fuller, Franklyn B.: Numerical Solutions for Supersonic Flow of an Ideal Gas Around Blunt Two-Dimensional Bodies. NASA TN D-791, 1961.
12. Zlotnick, Martin; and Newman, Donald J.: Theoretical Calculation of the Flow on Blunt-Nosed Axisymmetric Bodies in a Hypersonic Stream. RAD-TR-2-57-29 (Contract No. AF-04(645)-30), AVCO Res. and Advanced Dev. Div., Sept. 19, 1957.

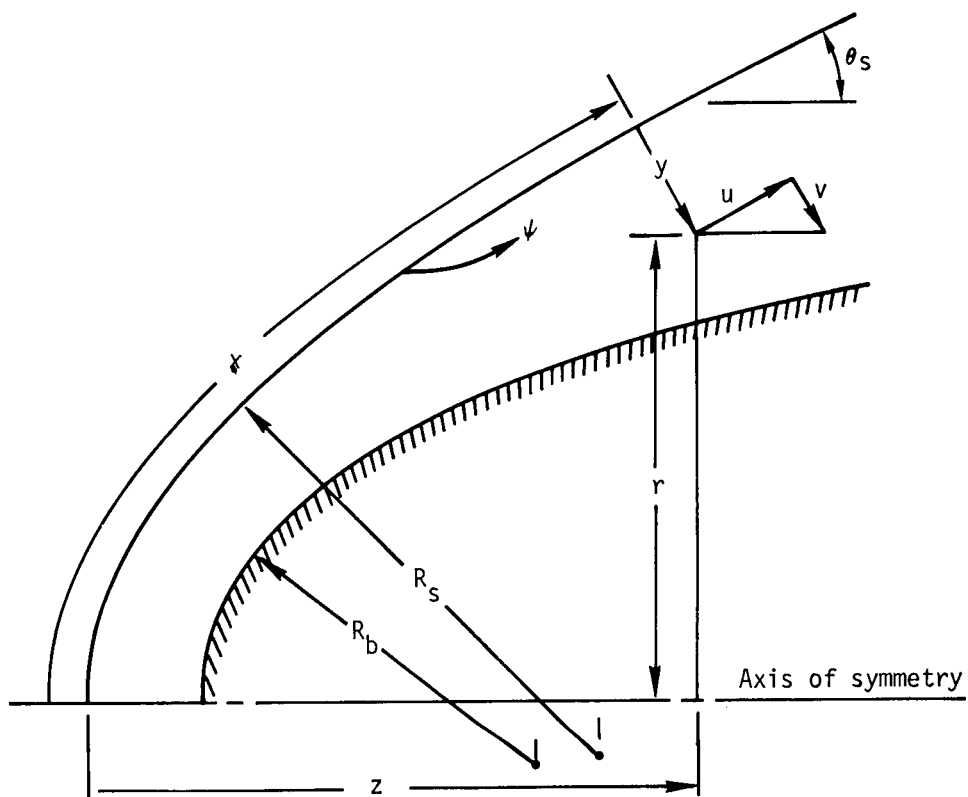
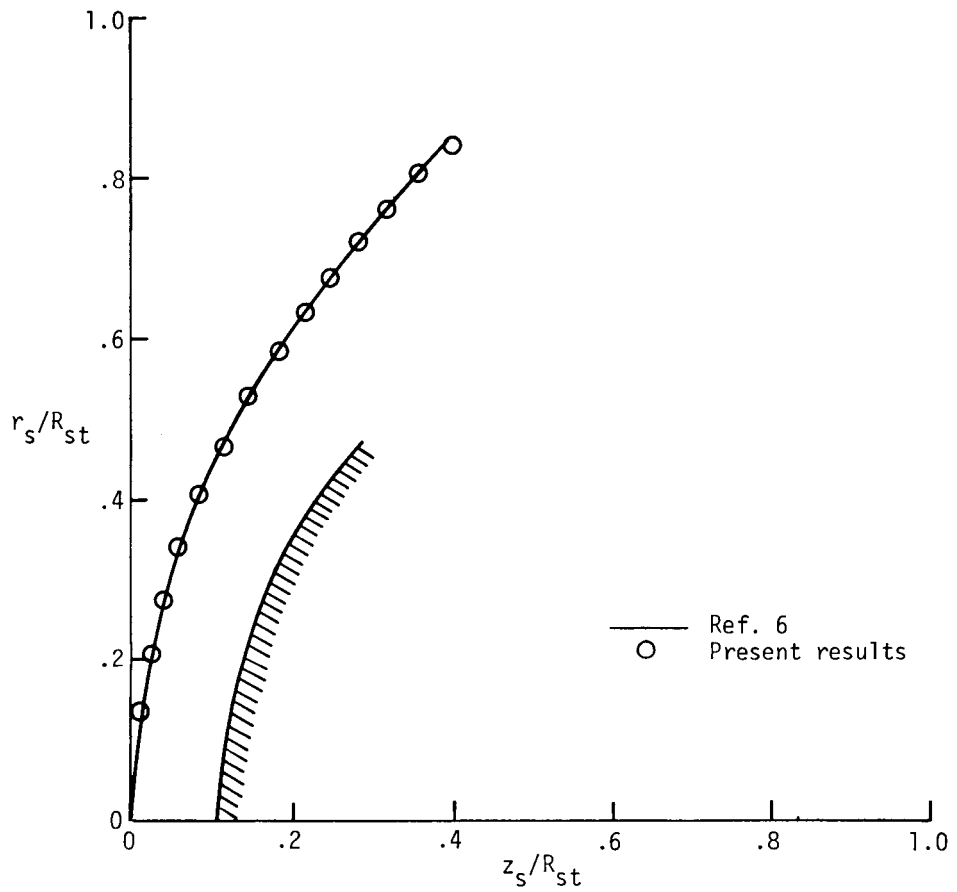
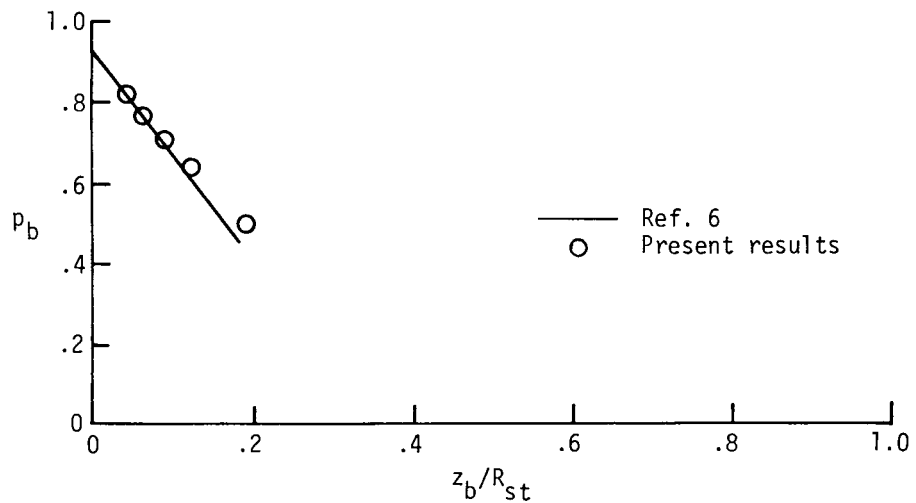


Figure 1. - Sketch of coordinate system.

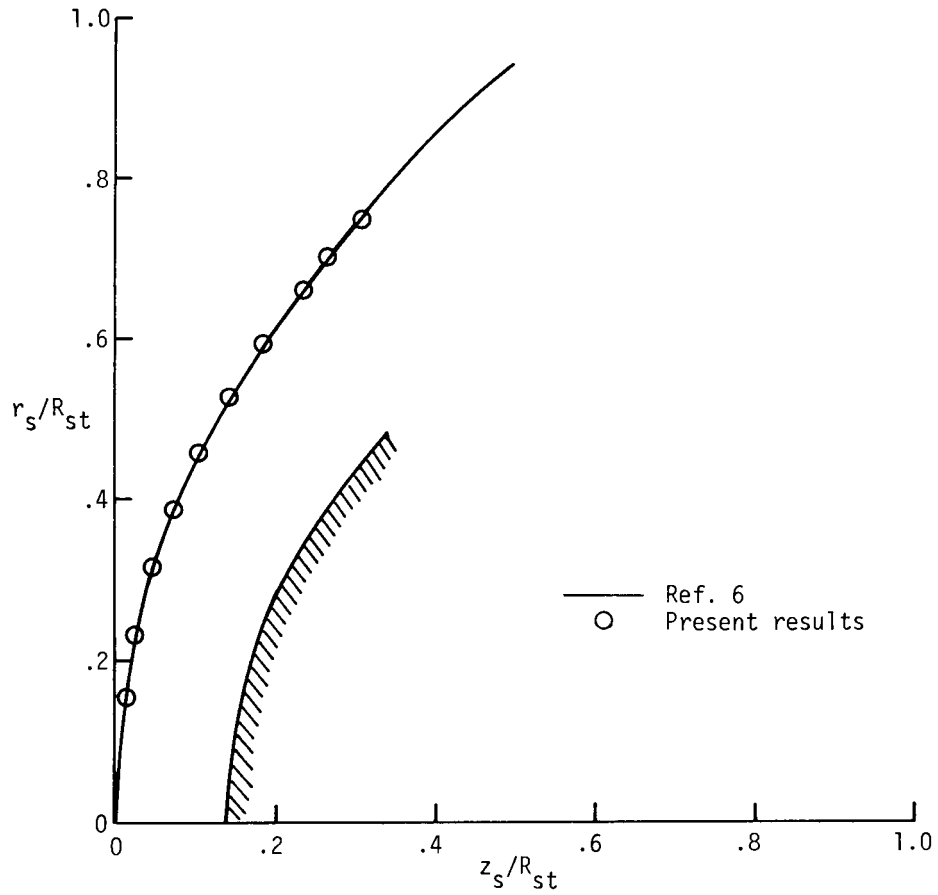


(a) Shock shape.

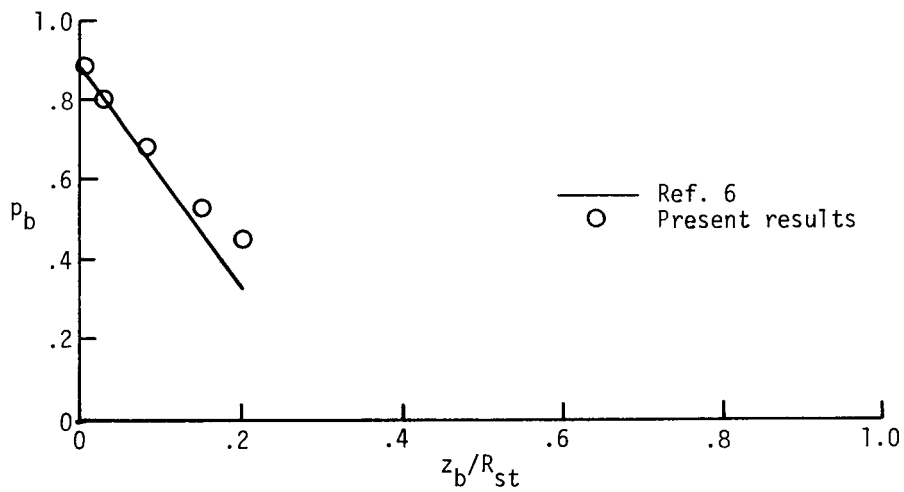


(b) Body pressure distribution.

Figure 2. - Comparison of shock shape and pressure distribution on sphere at $M_\infty = 6$ and $\gamma = 1.4$. $R_{st} = 1.34$.

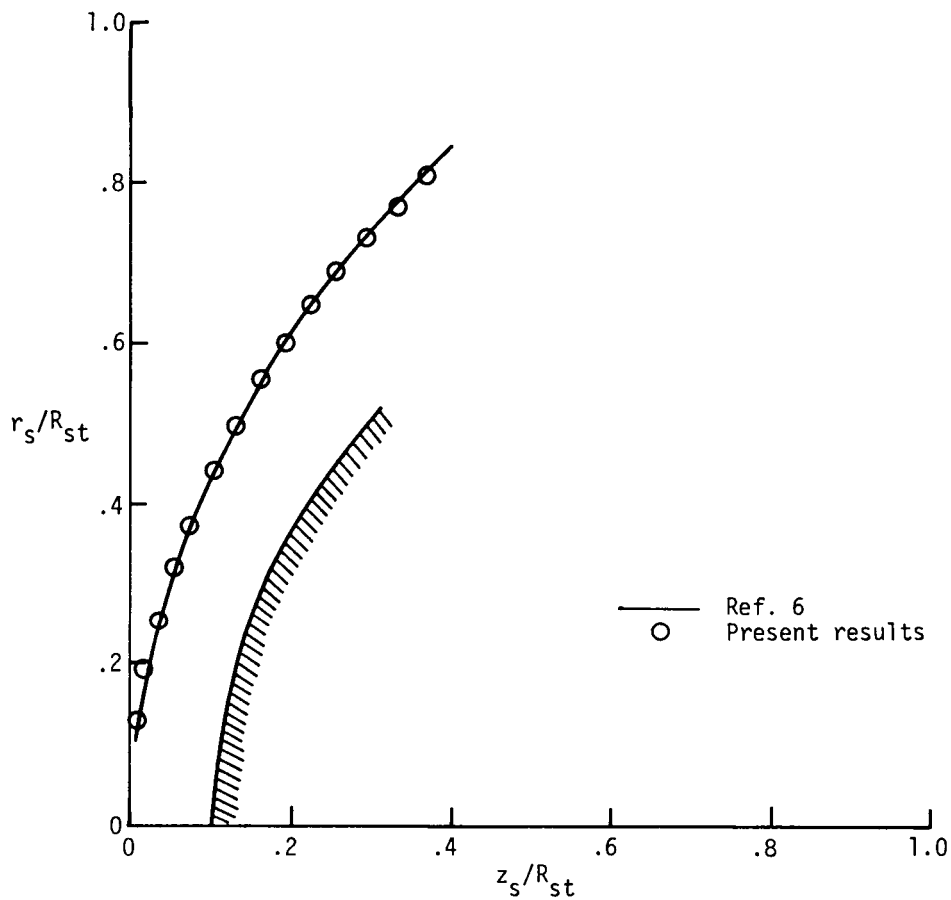


(a) Shock shape.

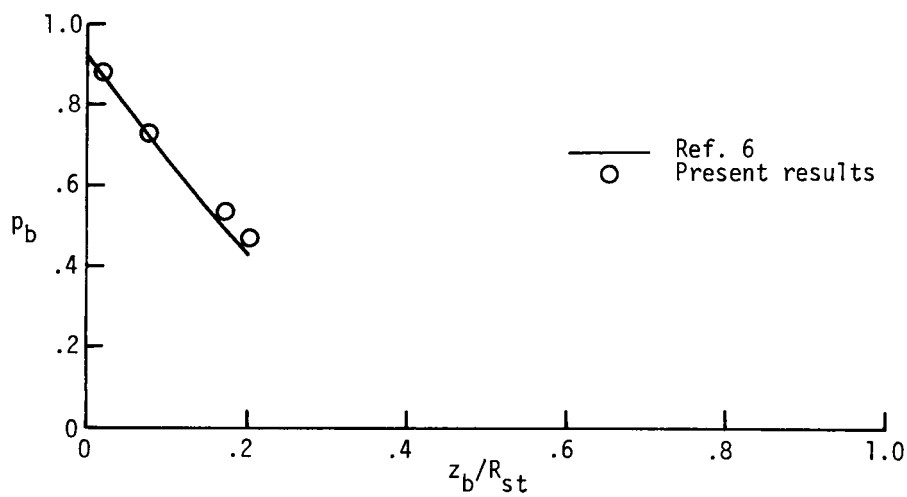


(b) Body pressure distribution.

Figure 3. - Comparison of shock shape and pressure distribution on sphere at $M_\infty = 10$ and $\gamma = 1.66$. $R_{st} = 1.43$.

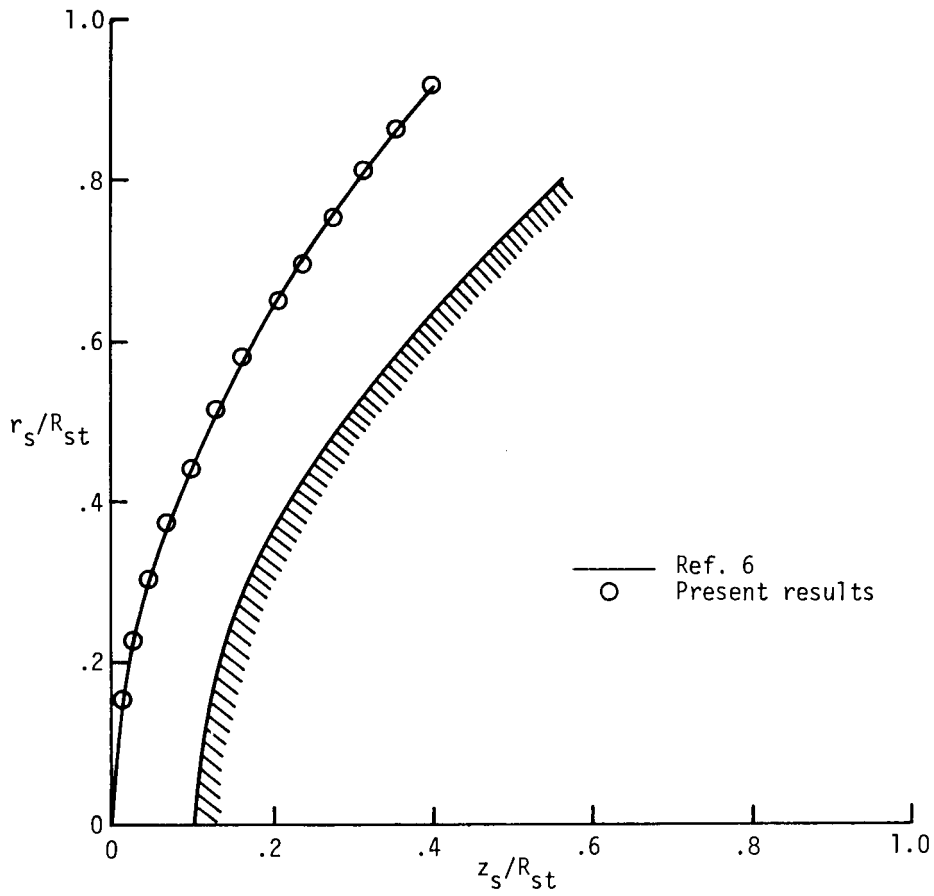


(a) Shock shape.

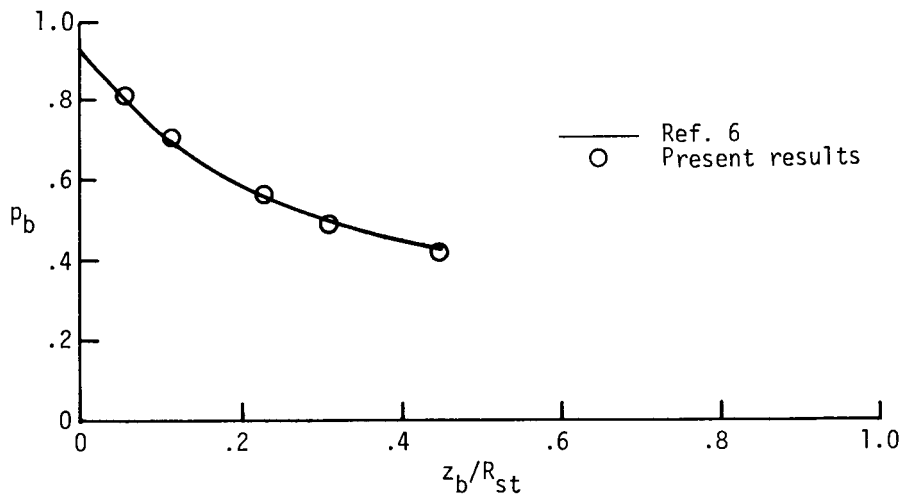


(b) Body pressure distribution.

Figure 4. - Comparison of shock shape and pressure distribution on sphere at $M_\infty = 10$ and $\gamma = 1.4$. $R_{st} = 1.3$.

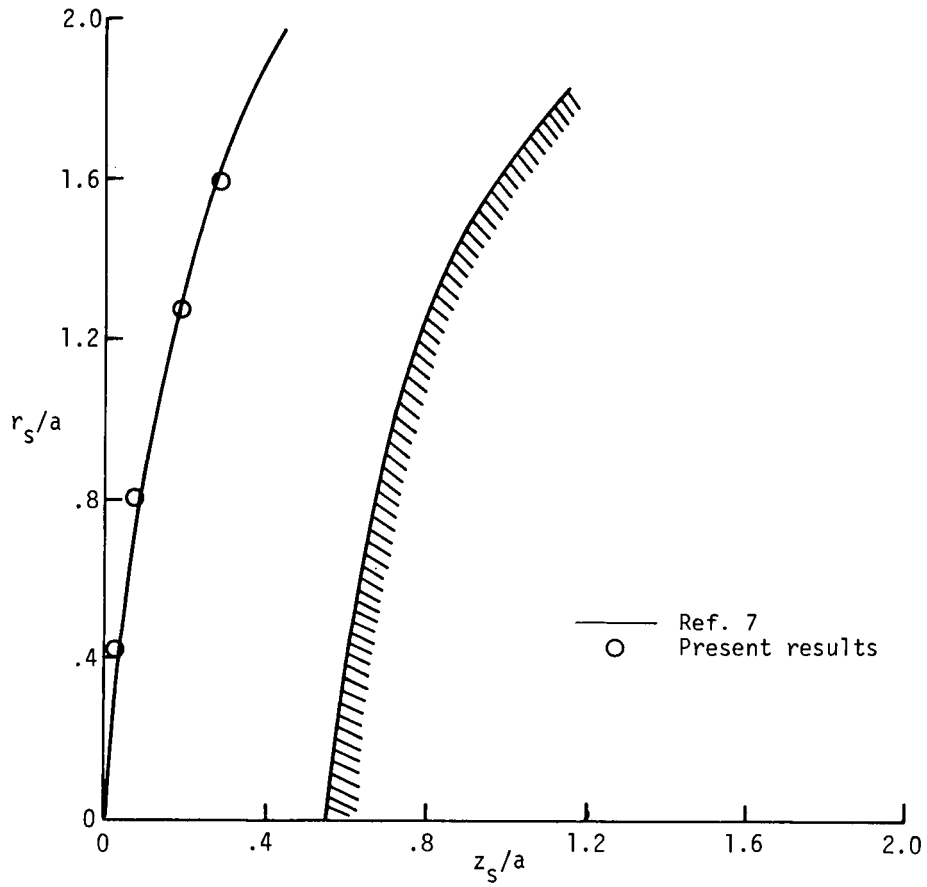


(a) Shock shape.

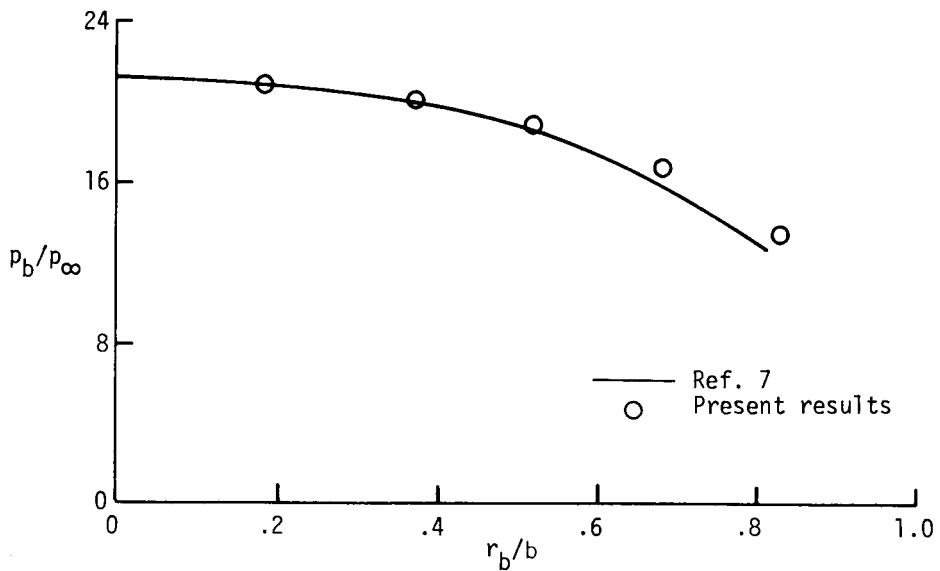


(b) Body pressure distribution.

Figure 5. - Comparison of shock shape and pressure distribution on paraboloid at $M_\infty = 10$ and $\gamma = 1.4$. $R_{st} = 1.42$.

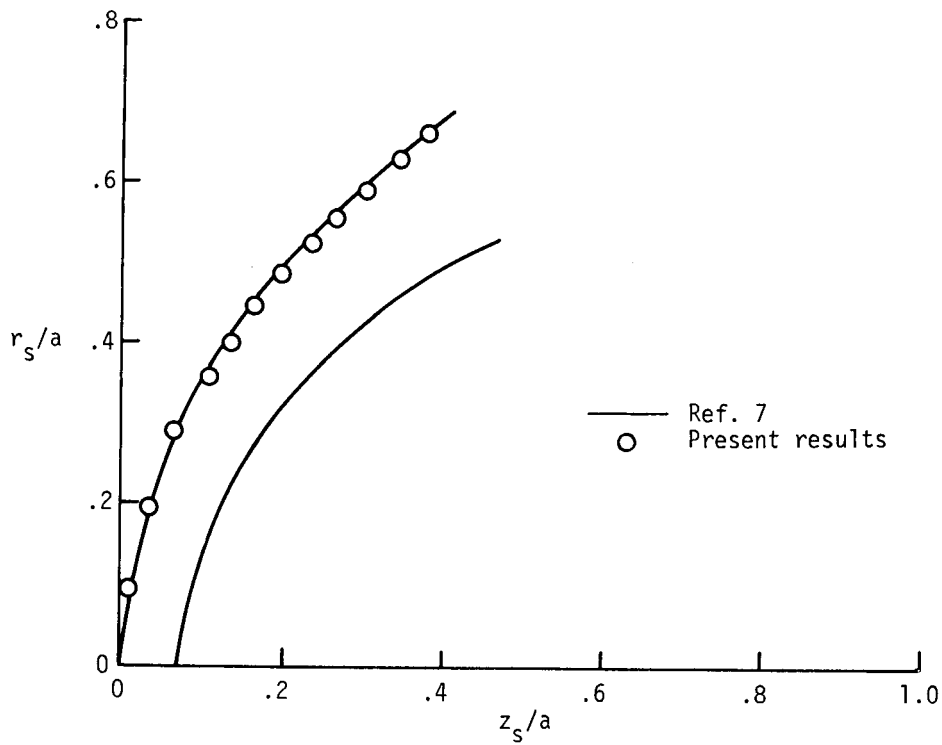


(a) Shock shape.

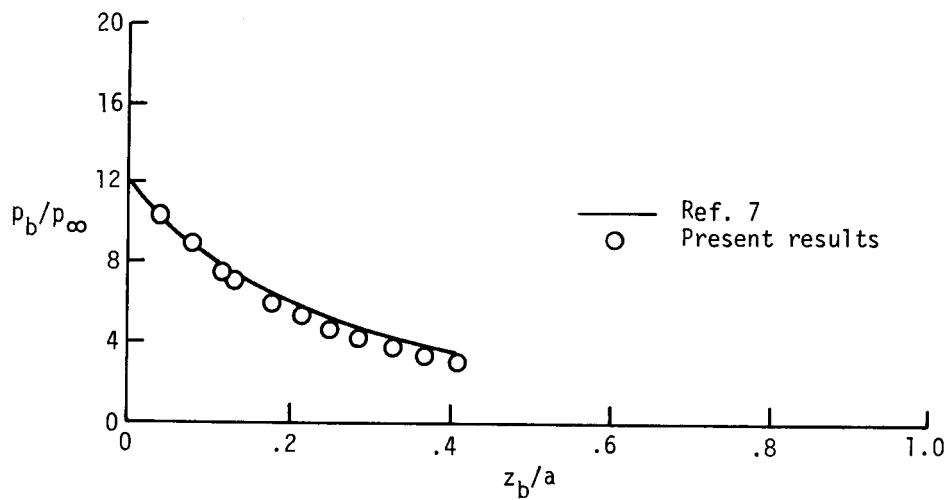


(b) Body pressure distribution.

Figure 6. - Comparison of shock and pressure distribution on 2/1 oblate ellipsoid at $M_\infty = 4$ and $\gamma = 1.4$. $a = 1.0$.

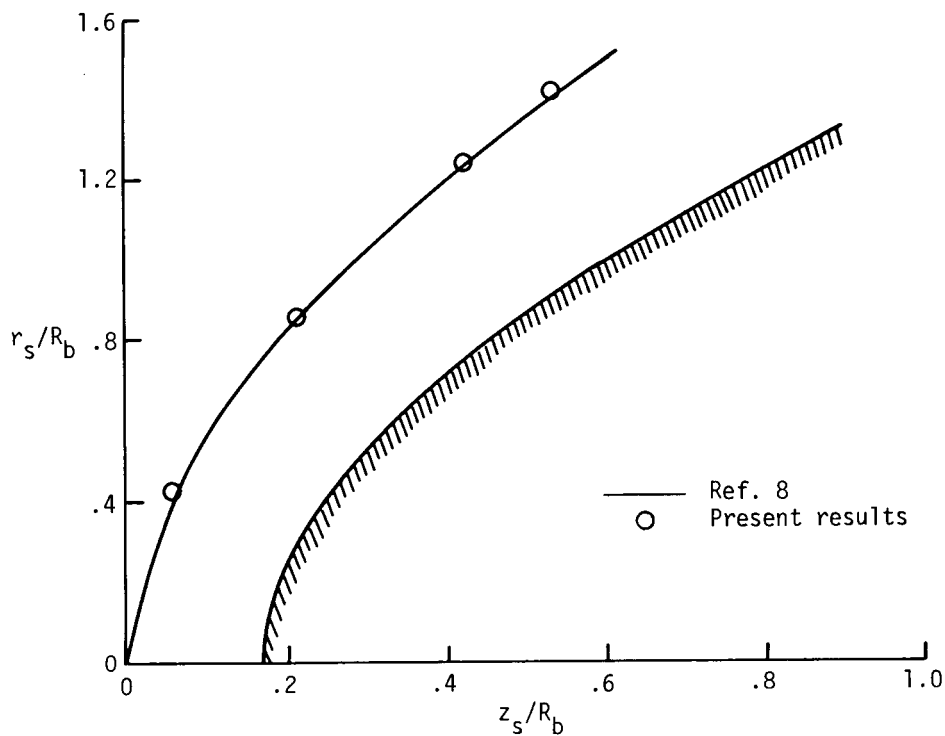


(a) Shock shape.

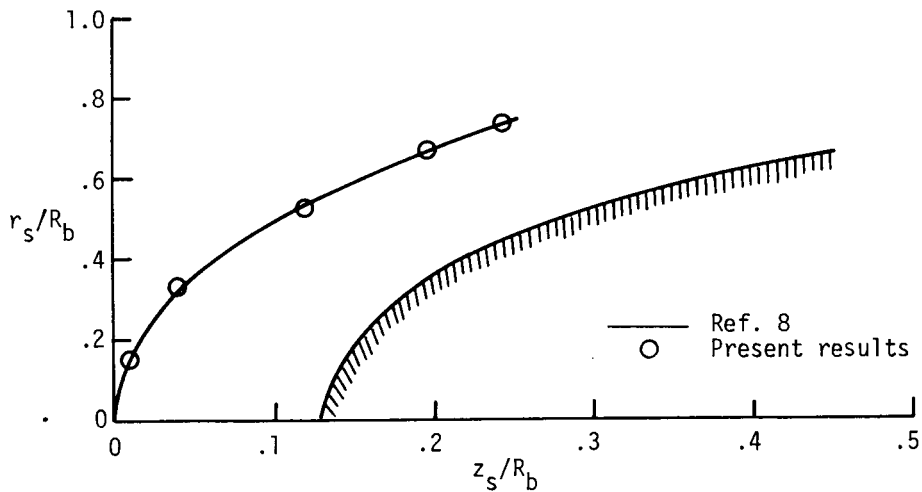


(b) Body pressure distribution.

Figure 7. - Comparison of shock shape and pressure distribution
on 2/3 prolate ellipsoid at $M_\infty = 8.08$ and $\gamma = 1.4$. $a = 3$.

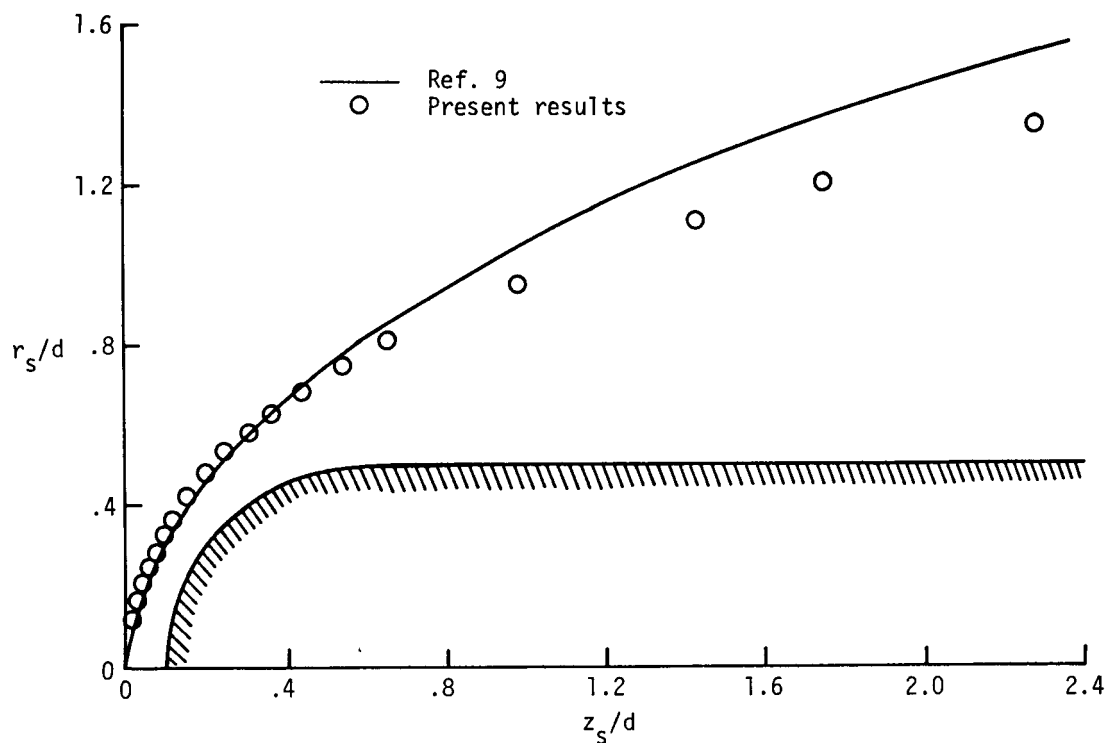


(a) Shock shape, hyperboloid. $R_b = 0.821$.

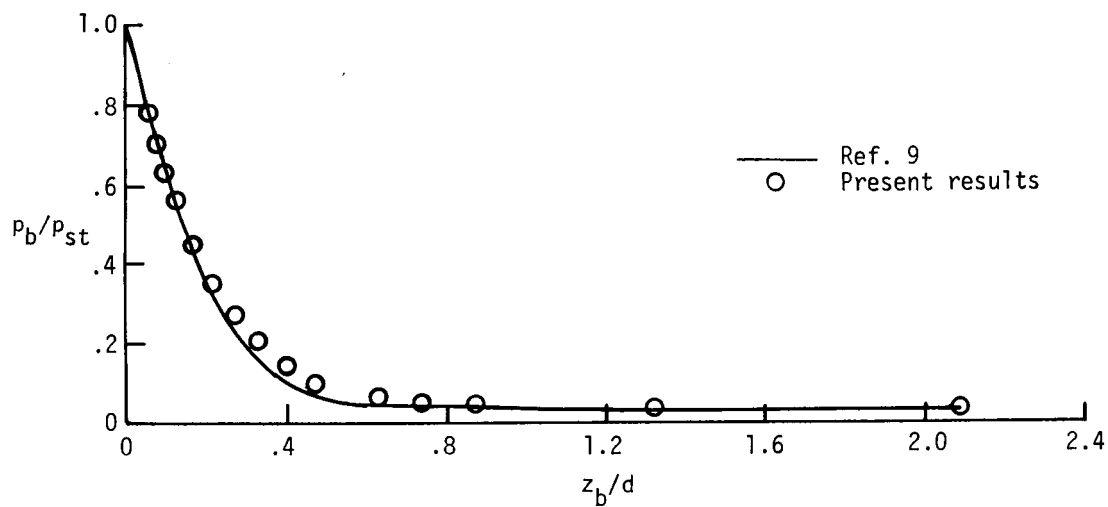


(b) Shock shape, oblate ellipsoid (1.414/1). $R_b = 2.0$.

Figure 8. - Comparison of shock shapes on blunt axisymmetric bodies at $M_\infty = 7$ and $\gamma = 1.4$.

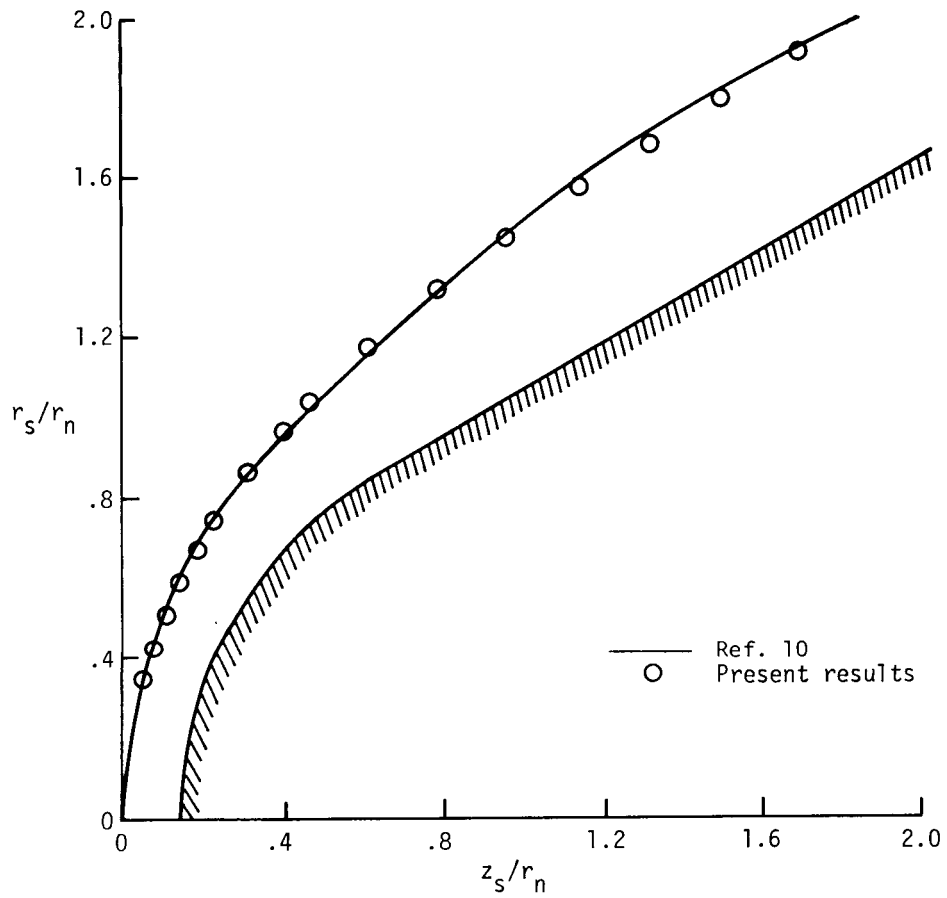


(a) Shock shape.

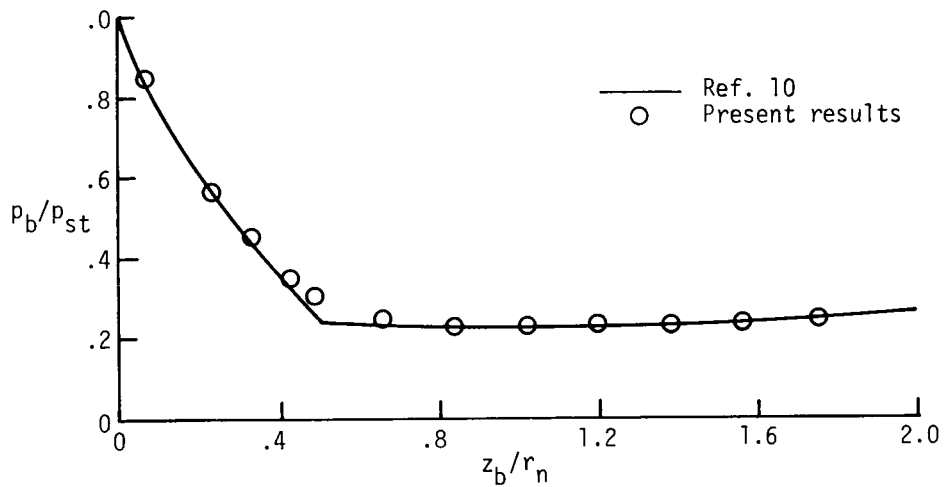


(b) Body pressure distribution.

Figure 9. - Comparison of shock shape and pressure distribution on hemisphere-cylinder at $M_\infty = 7.7$ and $\gamma = 1.4$. $d = 0.75$.

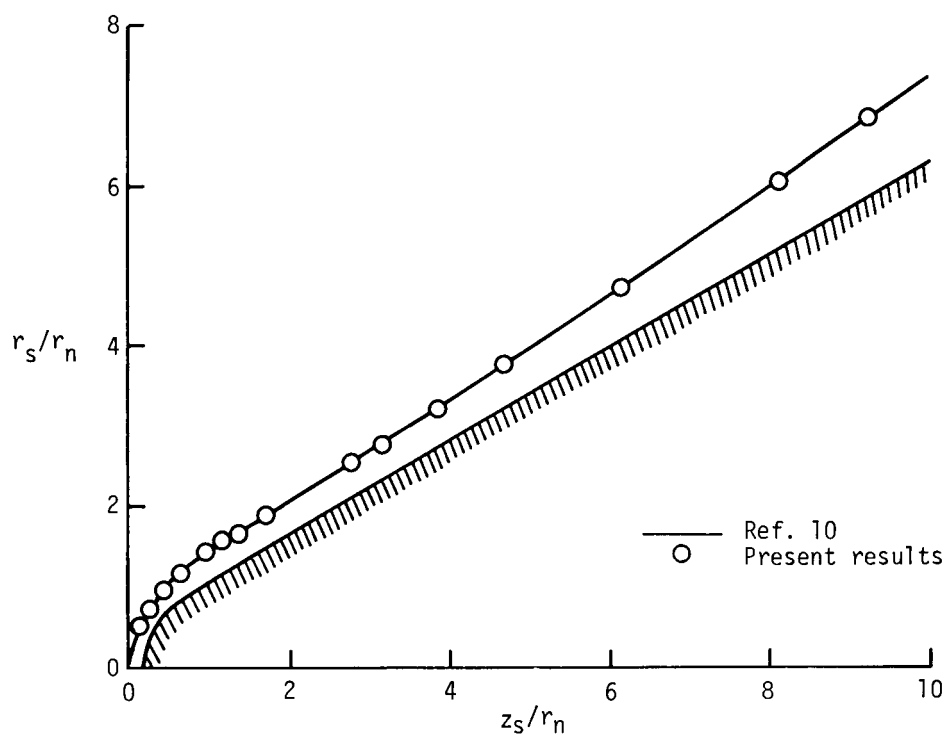


(a) Shock shape.

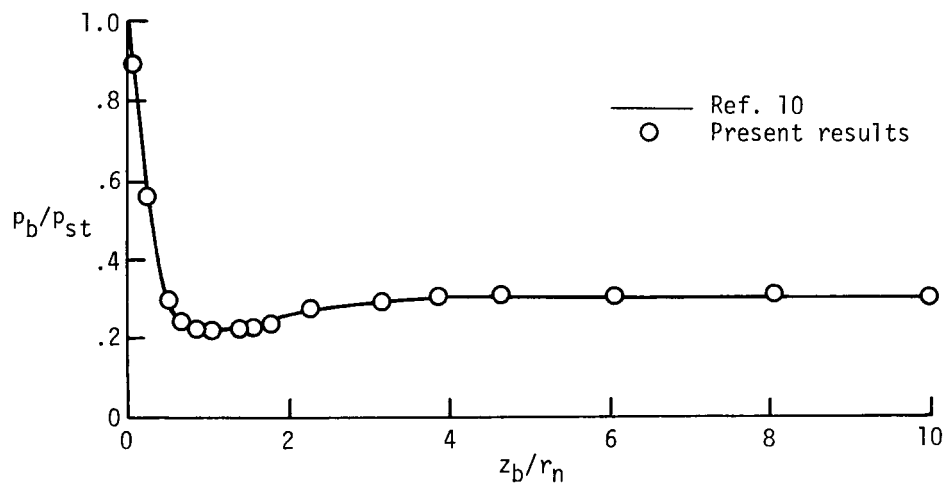


(b) Body pressure distribution.

Figure 10. - Comparison of shock shape and pressure distribution on spherically blunted 30° half-angle cone at $M_\infty = 8$ and $\gamma = 1.4$. $r_n = 1.0$.

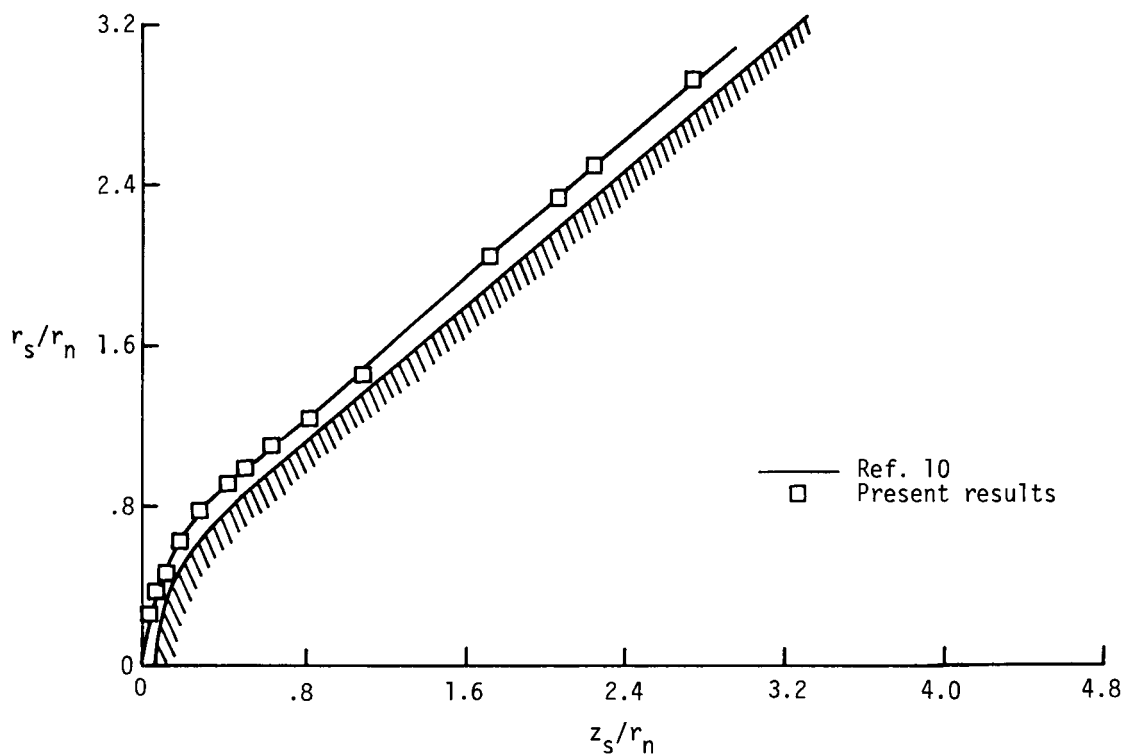


(c) Shock shape.

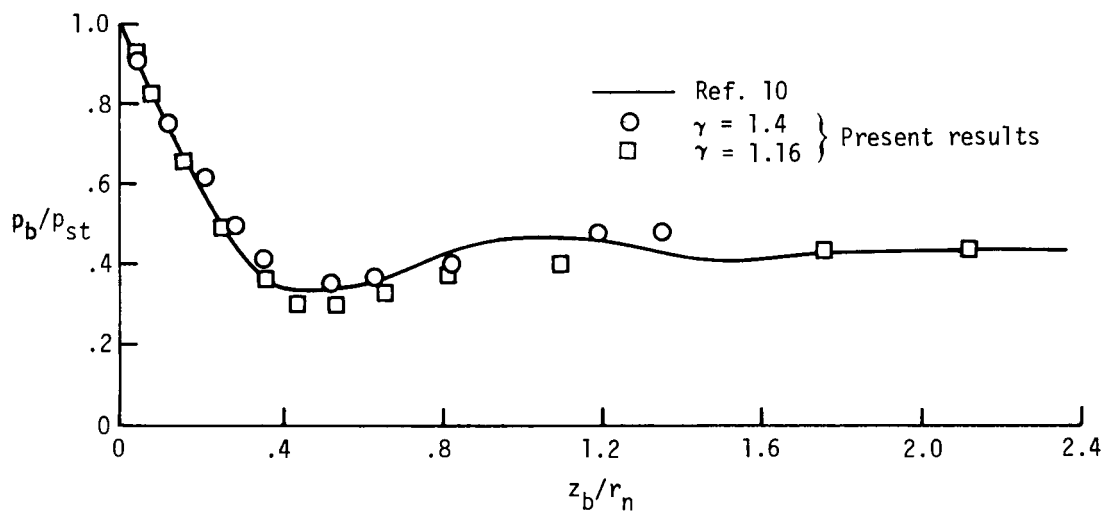


(d) Body pressure.

Figure 10. - Concluded.



(a) Shock shape ($\gamma = 1.16$).



(b) Body pressure distribution.

Figure 11. - Comparison of shock shape and pressure distribution on spherically blunted 40° half-angle cone at $M_\infty = 38.4$. $r_n = 1.0$.